DEVELOPMENT OF AUTOMOBILE CHASSIS PARTS VIA ALUMINUM
EXTRUSION AND SAND CASTING TECHNOLOGY

A THESIS SUBMITTED TO
THE GRADUATE SCHOOL OF NATURAL AND APPLIED SCIENCES
OF
MIDDLE EAST TECHNICAL UNIVERSITY

BY

ONUR DEMİREL

IN PARTIAL FULFILLMENT OF THE REQUIREMENTS
FOR
THE DEGREE OF MASTER OF SCIENCE
IN
METALLURGICAL AND MATERIALS ENGINEERING

SEPTEMBER 2012

Approval of the thesis:

DEVELOPMENT OF AUTOMOBILE CHASSIS PARTS VIA ALUMINUM EXTRUSION AND SAND CASTING TECHNOLOGY

submitted by **ONUR DEMİREL** in partial fulfillment of the requirements for the degree of **Master of Science in Metallurgical and Materials Engineering Department, Middle East Technical University** by,

Prof. Dr. Canan Özgen   _____
Dean, Graduate School of **Natural and Applied Science**

Prof. Dr. C. Hakan Gür   _____
Head of Department, **Metallurgical and Materials Eng.**

Prof. Dr. Ali Kalkanlı   _____
Supervisor, **Metallurgical and Materials Eng. Dept., METU**

Examining Committee Members:

Prof. Dr. Ekrem Selçuk   _____
Metallurgical and Materials Engineering Dept., METU

Prof. Dr. Ali Kalkanlı   _____
Metallurgical and Materials Engineering Dept., METU

Prof. Dr. Haluk Atala   _____
Metallurgical and Materials Engineering Dept., METU

Assist. Prof. Dr. Benat Koçkar   _____
Mechanical Engineering Dept. Hacettepe University

Dr. Caner Batıgün   _____
Welding Technology and NDT Center, METU

Date: 03.09.2012

I hereby declare that all information in this document has been obtained and presented in accordance with academic rules and ethical conduct. I also declare that, as required by these rules and conduct, I have fully cited and referenced all materials and results that are not original to this work.

Name, Last name: **Onur Demirel**

Signature   :

ABSTRACT

DEVELOPMENT OF AUTOMOBILE CHASSIS PARTS VIA ALUMINIUM EXTRUSION AND SAND CASTING TECHNOLOGY

DEMİREL, Onur

M.S., Department of Metallurgical and Materials Engineering

Supervisor: Prof. Dr. Ali KALKANLI

September 2012, 93 Pages

Due to the environmental issues related with fuel consumption and additionally passenger safety, aluminum space frame chassis is promising a big opportunity to design a lightweight structure with a high stiffness. Despite the lower stiffness and strength of aluminum in comparison to the conventional steel chassis, it can be compensated with changing thickness and design of structure by space frame geometry

In this study, instead of using steel for automobile chassis, main goal is producing a space frame structure with using aluminum in an extrusion and sand casting processes and improve the stiffness. Chassis is designed according to calculations for moment of inertia, torsional and bending stiffness and in sufficient structural stiffness which can compete with steel chassis. Static finite element analysis was carried out to understand the chassis bending, torsional stiffness and fatigue behaviors. For frontal collisions, dynamic finite element analysis was also done to

determine increases in the energy absorbance, specific energy absorbance and peak force for passenger safety.

Aluminum profiles were produced by hot extrusion and joined with sand casting parts by TIG welding to manufacture a space frame structure. For main chassis profile, 6063 series of aluminum alloy was selected due to availability for extrusion process, weldability and having sufficient tensile strength and percent elongation and treatment response. Three point bending test was carried out to determine flexural strength. Moment of inertia calculations were done. Some parts such as side frame and shock absorber tower were produced by sand casting method. A similar composition to Silafont – 36 aluminum alloy was selected because of its high fluidity and good mechanical properties; despite it is a die cast alloy. Tensile, hardness and Charpy impact test were conducted to determine the mechanical characteristics of Silafont - 36 sand cast alloy. In addition to microstructure features and thermal analysis were also carried out to achieve sufficient alloy properties. Heat affected zone was investigated by hardness and tensile test to determine the mechanical properties change after welding process.

In this space frame development study, A, B and C pillar parts were produced by Al – Si sand casting and T6 heat treatment then welded together by TIG welding and finally assembled on the bottom chassis frame produced by using 6063 extrudes welded by 4000 series electrodes.

The space frame chassis was studied by also computer simulation to test and see critical points which must be modified during manufacturing.

Besides the experimental and theoretical studies, space frame was also produced at the same time. According to the experimental results, the feasibility of the production of lightweight and solid chassis structure was achieved.

Key words: sand casting, extrusion, aluminum, FEA, space frame

ÖZ

OTOMOBİL ŞASİ PARÇALARININ ALUMİNYUM EKSTRÜZYON VE KUM DÖKÜM YÖNTEMİ İLE GELİŞTİRİLMESİ

DEMİREL, Onur

Yüksek Lisans, Metalurji ve Malzeme Mühendisliği

Tez Yöneticisi: Prof. Dr. Ali KALKANLI

Ekim 2012, 93 Sayfa

Yakıt tüketimiyle oluşan çevresel sorunlar ve yolcu güvenliği gibi sebepler sonucu alüminyum uzay kafes şasi yüksek katılık avantajı yanında hafifliği nedeniyle de tercih edilmektedir. Alüminyum, geleneksel çelik şasiye göre daha düşük katılık ve dayanıma sahip olmasına rağmen, uzay kafes tipi şasi üzerinde tasarım ve kalınlık değişikliklerine gidilerek benzer ihtiyaçları karşılayabilmektedir.

Bu çalışmada, otomobil şasisinde çelik kullanmak yerine, esas olarak alüminyum alaşımları kullanılarak ekstrüzyon ve kum döküm yöntemleriyle uzay kafes tipi şasi üretimi amaçlanmış ve katılık özellikleri geliştirilmiştir. Şasi, çelik yapıyı karşılayabilecek şekilde hesaplamalar yapılarak ve yeterli mekanik özellikler göz önünde bulundurularak tasarlanmıştır. Statik sonlu elemanlar yöntemi kullanılarak şasinin burulma ve eğilme özellikleri ve yorulma davranışlarının analizi yapılmıştır. Aynı zamanda önden çarpışmalardaki yolcu güvenliği için enerji emilimi, özgül

enerji emilimi ve azami kuvvetin bulunması amacıyla dinamik sonlu elemanlar analizi yapılmıştır.

Alüminyum ekstrüzyon profiller üretilerek kum döküm parçalarla birleştirilmiş ve uzay kafes tipi şasi elde edilmiştir. 6063 alüminyum alaşımı ekstrüzyona, kaynağa ve ısıl işleme uyumluluğu ve yeterli mekanik özellikleri nedeniyle tercih edilmiştir. 3 nokta eğme testi yapılarak enerji emilimi hesaplanmıştır ve buradan yola çıkarak atalet momenti hesapları yapılmıştır. Yan çerçeve ve amortisör kulesi gibi parçalar kum döküm yöntemiyle üretilmiştir. Silafont – 36 alaşımına benzer bir kompozisyon basınçlı döküm alaşımı olmasına rağmen yüksek akışkanlığı ve yüksek mekanik özellikleri nedeniyle seçilmiştir. Silafont – 36 kum döküm alaşımının mekanik özelliklerinin tespit edilebilmesi için çekme, sertlik ve Charpy darbe testleri uygulanmıştır. Buna ek olarak, doğru alaşım yapısının belirlenmesi için mikro yapı incelenmiş ve termal analizler yapılmıştır. Kaynak sonrası farklı ısıl işlemler ile ısıdan etkilenen bölgenin değişen sertliği incelenmiş ve kaynak dikişinin azami dayancını elde etmek amacıyla çekme testleri yapılmıştır

Deneysel ve teorik çalışmaların yanında aynı zamanda uzay kafes tipi şasi üretilmiştir. Deneysel sonuçlardan yola çıkılarak hafif, çevreci ve yüksek katılığa sahip aracın üretilebilirliği tespit edilmiştir.

Anahtar sözcükler: kum döküm, ekstrüzyon, alüminyum, SEA, uzay kafes

To my parents,

ACKNOWLEDGEMENTS

First of all I would like to imply my gratitude to my supervisor Prof. Dr. Ali Kalkanlı for precious encouragement, guidance and support from the beginning to the end of all our studies.

My special thanks go to the technical staffs of the Department of Metallurgical and Materials Engineering, METU, especially Salih Türe and Cemal Yanardağ for their contributions to this study.

I would also like to express my thanks to my friends and colleague who are Ümit Akçaoğlu, Murat Kamberoğlu, Kıvanç Korkmaz, Elif Selen Ateş, Eylem Kahramansoy, Işık Yılmaz Okçu, Ozan Muştak, Mehmet Tümerkan Kesim, Hakan Yavaş, Göksu Gürer, Şerif Kaya, Güher Kotan and Evren Tan for morale and courage given by them.

Thanks are also extended to Deniz Taşkesen who is head of the RUTAŞ® Co. and Dr.Caner Batıgün who is academic studies and R&D officer in Welding Technology, METU.

Finally, the biggest and the most sincere gratitude should be expressed to Candan Demirel, Sevim Demirel, Okan Demirel and Deniz Erbay for their unconditional supports.

My thesis was founded by SAN-TEZ project signed between Ministry of Science, Industry and Technology of Turkey, Malkoçlar Oto and Middle East Technical University.

TABLE OF CONTENTS

LIST OF FIGURES

FIGURES

LIST OF TABLES

CHAPTER 1

INTRODUCTION

In recent years, weight reduction is one of the most important parameter in automobile industry because of the importance of the energy saving. Providing fuel saving prevents CO_2 emission which is an important issue for environment. Moreover, reduction in fuel consumption insures economic benefits. On the other hand, passenger safety is also a crucial criterion while designing an automobile. Therefore, automobile manufacturers have struggled to ensure a safe drive with a higher performance while reducing the weight safety.

Due to the reasons mentioned above, light metals are promising a big opportunity in decreasing the total weight of a car. Using aluminum alloys provide $30 - 40\%$ lighter automobile body when compared to steel. Despite the lower stiffness and strength of aluminum in comparison to the conventional steel chassis, it can be compensated with changing thickness and design of structure to a space frame geometry. Also the number of parts and welding sections can be reduced. In an aluminum space frame, straight extrusion profiles and complex casting parts are joined together to create a rigid structure. The behavior of chassis against static and dynamic loadings must be in safety region while designing a rigid structure.

According to the government support for national automobile production and developments for an electrical vehicle nowadays, no attempts were made ever before with using aluminum to produce a space frame chassis in Turkey. The aim of this study is to investigate the production of aluminum space frame for an electrical vehicle with a small amount of budget. Due to economic reasons, sand casting method was selected instead of die casting which is also the main difference from the

other studies. Although many workouts were done before in manufacturing side frame of chassis by die cast and extruded parts, still all side parts were manufactured with sand casting process in our study, which is the only example in literature. Silafont – 36 was selected as a proper aluminum alloy and mechanical properties in sand casting were investigated without noticing its being a die cast alloy.

This study was carried out in two stages; in the first stage, the design of steel monocoque chassis of a sedan car was revised to the aluminum space frame. While modeling the space frame chassis, design and some other criterions were inspired from major car manufacturers in Germany and Italy. In our study, space frame chassis type was selected specifically in order to improve the stiffness of total structure and to maintain these properties during driving. Chassis design was developed to provide sufficient stiffness against static loadings. Crashworthiness was also investigated to determine the energy absorption capability of chassis in terms of the protection of occupants during frontal impact. Weak joint parts after welding were also identified and strengthened. Lastly, Dynamic (explicit) and Static (implicit) Finite Element Analyses were utilized to detect chassis behavior against different loads which cannot be measured in laboratory environment because of time and cost limitations.

In the second stage, chassis was manufactured with the help of the design optimization. In order to select proper alloy and production method, many examinations were investigated. Thermal analysis and micro investigations (light microscopy, EDX) of sand casting were carried out to maintain sufficient modifications. Mechanical tests were also held to evaluate the proper heat treatment and the quality of welding sections.

CHAPTER 2

THEORY AND LITERATURE SURVEY

2.1 Aluminum in Automobile

Due to environmental factors and economic issues, car manufacturers are considering many solutions and making researches to decrease fuel consumption. As well as this, improvement in luxury and comfort, performance and safety systems in new generation automobiles gives extra weight to the vehicle. [1] The easiest way to increase fuel saving is to reduce the weight of automobile. Weight reduction of a car by 10% results approximately %5.5 improvement in fuel saving. [2]

Therefore, aluminum becomes an important material for manufacturers. Owing to its low density, a light-weight chassis and car parts can be produced and fuel economy is provided. Starting with 110 kg in 1996, the usage of aluminum in car is estimated to increase up to 350 kg in 2015. [3]

Apart from economic benefits, reduction in fuel consumption decreases CO_2 emission which is the main problem of global warming. [4]

Use of aluminum enables to obtain light- weight structure, in which aluminum shows the sufficient mechanic properties as steel. So, there is no change in passenger safety while gaining an advantage of strength is gained to weight ratio over steel. [5]

2.1.1 Advantages

- Light-weight: Due to its low density compared to steel, approximately 30-40% weight saving is obtained. As a result of that, total weight of vehicle is reduced, load capacity is increased and fuel economy is provided.

- Energy Absorption: For safety of passengers during the crash, occupant's cabin must be enough strength. Additionally, front, rare and side frames need to absorb enough energy and not to transmit to the passengers. Compared to the other traditional metals, with proper alloy and heat treatment selection, buckling occurs in a controlled manner during crash and more energy absorption is achieved. [6]

- Design Flexibility: Due to high extrudability of aluminum, more complex parts can be produced rapidly. Several steel sheets are eliminated in assembly by using simple closed tubes that are ready in one process by using aluminum. [1] As a result of this, production is accelerated with fewer parts, assembling process becomes easier and more working spaces are saved. Using aluminum reduce number of components by 25 % in place of traditional steel structure.

- Recyclability: There is not any quality loss while using an aluminum scrap and only 5% energy input is needed in recycling process compared to primer aluminum production. In recent years, with increasing aluminum usage, 30 – 50 % of automobile parts can be recycled. [6]

- Corrosion Resistance: Due to its natural oxide coating, connection is cut off with environment and does not require any additional protection like steel. Oxygen, other gases and liquids cannot pass through this tough and thick layer on surface. [7]

- Apart from these; more rigid body is obtained, the center of gravity lowers and handling and driving characteristics are improved [5]

2.1.2 Disadvantages

- Young's Modulus: In comparison of Young's Modulus between steel and aluminum, there is a ratio as 1/3. While Young's Modulus of steel is 206 MPa, aluminum is 69 MPa. This means, in same design criterion, aluminum structure will deflect 3 times more than steel structure. In order to compensate the same stiffness as steel, design and thickness of cross-section in aluminum structure should be changed. [1]

- Cost: A rule of thumb, a material cost of aluminum is more expensive than steel. So, parts that are produced with aluminum appear a cost penalty. But, aluminum can be recycled and if we take into account the steel stamp tooling costs, this situation becomes balanced. Also, design flexibility eliminates unnecessary processes to obtain the final product. When compared, stamp dies are again more expensive than extrusion dies. Aluminum is inexpensive material for manufacturers in volumes of production under 100,000 cars per year. [8]

- Welding: Heat treatable aluminum alloys lose their hardening properties, especially in HAZ, after welding. Compared to steel, aluminum shows lower hardness and strength characteristics in HAZ. Additionally, during welding process, there is a risk of hot cracking. This situation depends on alloy, temper and welding selection. [9]

2.1.3 Space Frame Technology

Aluminum space frame is one of the major developments in chassis technology nowadays. In this technique, straight and curved closed sections that are produced by extrusion process are connected together in corners and joint parts, with the help of complex cast parts to create a rigid structure. [4]

There are some requirements in aluminum space frame;

- Weight as low as possible,
- Stable passenger cabin, least damage must be consisted after accidents,

- Sufficient rigidity,
- High static torsion strength, combined with light-weight to optimum driving safety,
- High corrosion resistance,
- Weldable,
- Suitable for recycling

Extruded profiles eliminate many large pressed parts and reduce total number of components. Profiles that are used in front, rare and side frames are welded properly together and energy absorption increases by 50% in structure during crash compared with steel. Extrusions having individual wall thickness assure enough bending stiffness requirements. According to the use of complex cast parts in structure, weight reduction by 50% can be provided and several steel pressed parts are eliminated. Also, in corner and joint areas which are highly stressed zones, casting offers a contribution in sufficient connection between extrusion frames. [9]

2.2 Sand Casting

Sand casting is mostly used casting technique in producing large parts economically. In this method, patterns are used to form a desired cavity in sand, called mold, and molten metal is poured into this preformed cavity. Tooling costs makes sand casting more preferred instead of die casting for small investments. Because wood or plastic used as the pattern material in sand casting, is far easier to modify than the metal used for die casting.

2.2.1. Al-Si Alloys

Due to their excellent casting properties, Al-Si alloys are most widely used aluminum alloys in automotive, military and structural parts. Besides its high level of fluidity, which can be obtained maximum in eutectic composition, desired mechanical properties are also achieved. [10]

Concentration range of Si varies between 4-22%. This range is divided into three sub-ranges; hypoeutectic (4-9% Si), eutectic (10-13% Si) and hypereutectic (14-22% Si). Microstructure of eutectic Al-Si alloys (AlSi12) mainly includes small amounts of primary (Al) dendrites and primary (Si) crystals.

The major alloying elements of Al-Si alloys are Si, Cu and Mg. Simply alloying elements increase strength and hardness, while reducing elongation. The effects of elements are stated below;

- Si: Silicon is the main alloying element, which provides high fluidity, low shrinkage and improvement in hot tear resistance and weldability characteristics. [11] With a high feeding behavior, casting of complex parts and thinner sections becomes easier. Because of the segregation tendency of Si to the grain boundaries, ductility is reduced and it causes intergranular embrittment

- Mg: The Magnesium addition is increased strength and hardness characteristics in heat treated Al-Si alloys. Also increasing magnesium content in aluminum has a negative influence on ductility by increasing precipitates. Mg content is selected according to the desired mechanical property; for high strength 0.3-0.4% Mg, for high ductility 0.15% Mg. Higher strength cannot be obtained above 0.5% because excess Mg is precipitated as Mg_2Si. [12] Due to its low density compared to aluminum, magnesium tends to float over the melt which increase the risk for dendritic oxidation. [13]

- Cu: Besides development in strength with addition of copper in Al-Si alloys, it decreases ductility and toughness. [10]

- Fe: The addition of iron allows a development in strength but also decreases the ductility on a large scale. For this reason iron is the most common impurity and above 0.7% iron content is not desired in Al-Si alloys. Because of very low solubility of iron (0.04%), excess iron form as an intermetallic second phase. This insoluble phase cause the embrittlement of the microstructure. The major intermetallic compound is $FeAl_3$. [14] These phases, which are the reason of starting point of cracks and tearing due to

morphology under the dynamic load or deformation, cause low strength and elongation with hindering the movement of dislocations. [12]

- Mn: Manganese is an impurity and no benefits in aluminum sand casting. Due to this reason the manganese content is desired in a minimum level. It tends to combine with iron to form insoluble phases. [15]

- H: Hydrogen is the only gas that has high solubility in aluminum in the liquid state. It comes from humidity of the atmosphere and its solubility is increased rapidly with increasing temperature. It reacts with aluminum; $3H_2O + 2Al$ » $3H + Al_2O_3$ and oxide layer is occurred. This thin layer does not allow oxygen to diffuse into the melt. Also Argon or Nitrogen is using to prevent this diffusion. These gases are dissolved in the melt with their fine bubbles and form a stable nuclei to reaches a partial equilibrium with the H_2. Than these saturated bubbles rise to the surface and H_2 burns. [13]

In automotive industry 3xx and 4xx aluminum casting alloys are generally preferred. A356.0 is one of the most widely used aluminum alloy due to its excellent casting properties. Also desired mechanical and physical properties can be achieved after artificial aging for military, automotive and aerospace parts. [11]

On the other hand, a special alloy combination that is called Silafont – 36, a trademark alloy by Rheinfelden (Germany), is also used in automotive chassis parts. It is suitable for lower wall thicknesses, excellent machinability and weldability. After heat treatment, higher elongation and energy absorption are also achieved in parts. For high deformation and easy forming, iron content is kept low as much as possible in this alloy to prevent AlFeSi phase in the microstructure. Magnesium is selected between 0.24-0.35% under conditions for parts requiring high strength and impact resistance.[12]

2.2.2 Grain Refinement

Advanced mechanical properties, homogeneity in microstructure, reduction in macro porosity and resistance to hot tear are results of the implementation method of grain refinement. In Al-Si alloy casting, grain refinement increases mass feeding that

causes reduction in shrinkage and finer porosity dispersion is stimulated. At the same time, fine grain size makes secondary intermetallic phases more uniform in addition to pores that are dissolved in the liquid. Because these brittle intermetallic compounds and porosity align between coarse grains and decrease the ability of elongation perpendicular to the grains. [16]

Grain refinement has an important effect on mechanical properties such as strength and ductility with changing distribution of secondary phase particles. With semi solidus temperature lowers, hot tearing tendency is reduced. Because of a shorter temperature range for hot tearing, casting gain strength at a faster rate. [17]

The objective of grain refinement is to enhance nucleation number in the melt and obtain finer grain sizes. This is achieved in two ways;

- Rapid cooling
- Addition of chemical grain refiner to the melt

With rapid cooling, smaller dendrites are formed with more number of nuclei in the casting and large undercooling may be obtained for starting of solidification. On the other hand, when master alloys or fluxes are added into the melt which are effective nuclei, solidification proceeds in very small undercooling. Despite the fact that it does not have much effect on the mechanical properties as rapid cooling; chemical grain refinement improves mechanical properties and leads to a fine porosity distribution. For Al-Si alloys, additions of grain refiner is more effective before modification [18]

Titanium is commonly used in chemical refinement of aluminum alloys. In general, titanium and aluminum create a $TiAl_3$ compound for heterogenic nuclei points in aluminum liquid. Added as a grain refining master alloy that has many $TiAl_3$ intermetallic inside, are distributed in liquid. $TiAl_3$ begins to dissolve in aluminum liquid and aluminum start to enrich with titanium after coming in contact with the particles. Due to higher liquidus temperature than base metal, titanium-rich liquid around the particle starts to solidify first. Sufficient titanium content ($>0.15\%$) is required to create primary aluminum first crystals in liquid metal, otherwise master alloy dissolve quickly and lose its effectiveness. Excess Ti addition form Ti intermetallics which reduce mechanical properties [19]

9
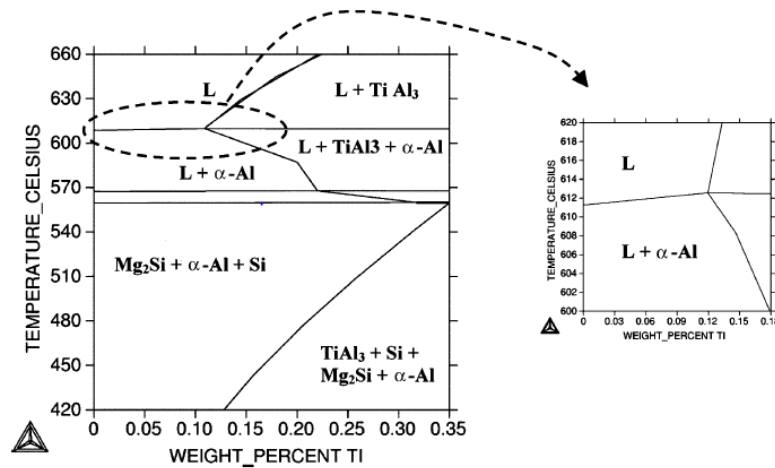
Figure 1: Pseudo – binary phase diagram of aluminum – titanium of A356.0 [20]

As in pseudo-binary phase diagram of Al- Ti, peritectic reaction occurs in lower Ti concentration and higher liquidus temperature. (Figure 1) From this, titanium addition takes nucleation start temperature to the higher points. Thermal analysis of grain refinement by Ti addition is also important to figure out the effectiveness. When we examine cooling curve of casting without grain refinement, undercooling must be done for nucleation by itself. But with grain refinement, nucleation starts over growth point and undercooling becomes less. (see Figure 2) [20]
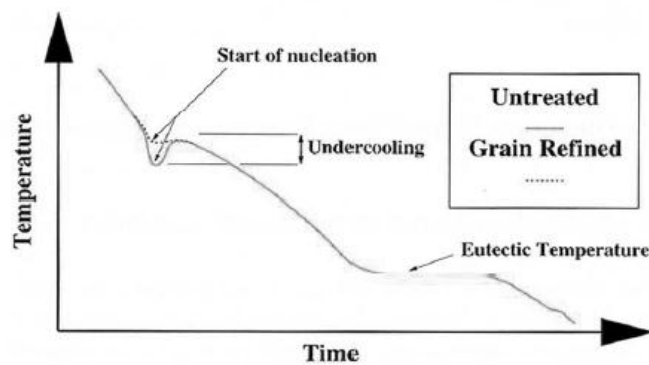
Figure 2: Comparison of cooling curves between untreated and grain refined aluminum alloy [21]

Because of dissolution problem of Ti, Boron is added to the liquid aluminum to improve refining effectiveness. Common master alloys contain Ti and B, in a ratio of 5 to 1. TiB_2 is not soluble in liquid aluminum, for this reason refining effectiveness

10

continues with more waiting time. Peritectic reaction takes place at higher temperatures and lasts shorter with a little undercooling. TiB_2 shifts the cooling curve up and nucleation starts around $TiAl_3$ spontaneously and grow very quickly. $TiAl_3$ plays an important role in nucleation with a help of TiB_2. After solidification, while $TiAl_3$ is involved inside the grain, boron particles stay in grain boundaries. [17]

2.2.3 Modification

Modification in eutectic alloys is mostly important at improving ductility properties compared to unmodified alloys. Besides increasing elongation, higher tensile properties are also achieved. Modification is more effective on elongation when the iron content is low. As a comparison in eutectic composition, while tensile strength is 150 MPa and elongation is 5% in unmodified alloy, values become 210 MPa and 12% respectively after modification. [12, 18]

Sodium and strontium are widely used as a master alloy in modification. Because of vaporization and oxidation problems, the addition of sodium cannot be controlled in liquid. This leads over or insufficient modification in casting. In this reason, strontium is more preferred as a modified element but strontium addition must be in controlled to be at low levels as a range of 0.008 − 0.04%. Modified alloy does not require re-modification in next casting because strontium loss is less and microstructure is preserved. [22] Strontium contains 10% in aluminum-strontium master alloys. If master alloys have higher strontium content, it has no modifying effect on casting because of containing aluminum and strontium intermetallics. On the other hand, higher additions increased the tendency of hydrogen solubility which is associated with increase in porosity [11]

Slow solidification rates in Al-Si alloys creates coarse and irregular shaped silicon particles. Because of brittle characteristics of coarse silicon, ductility is very low in this type of eutectics. The addition of strontium lowers eutectic temperature as 12 ºC and shifts the eutectic composition to the higher silicon side. (see Figure 3) This increase the nucleation rate and growth temperature of the eutectic is suppressed which results finer fibrous micro structure. Significantly little magnesium addition to

the aluminum matrix causes Mg$_2$Si precipitation and with a proper heat treatment, tensile strength increase substantially. This process is described in section 2.4 [23]
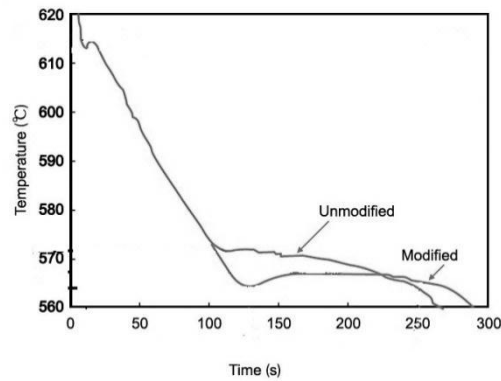
Figure 3: Comparison of cooling curves between unmodified and modified A356.0 aluminum alloy [54]

2.3 Extrusion

Simply, extrusion is a deformation process that a material is preheated at about 450-600ºC and pushed through steel die with a high pressure to form a profile with a desired cross-section. Easily forming complex shapes and high productivity is the main advantages of extrusion process. In this reason, it is the most common production for aluminum. In this process, almost any cross-sections can be produced within the die and pressure limits. Various mechanical properties can be achieved with a proper alloy and design selection. [13, 15]

2.3.1 Al-Si-Mg Alloys

Also known as 6xxx aluminum alloys contain magnesium (0.5-1.1%) and silicon (0.8-1.4%). Due to other impurities (Fe, Cu, Mn, Zn) in composition, profiles can be provided in different properties. Because of their excellent extrubility properties, Al-Si-Mg alloys are the first choice in extrusion process to produce profiles for

automotive industry, architecture and structural members. Through heat treatment process, demanded strength and stiffness can be obtained. Also 6xxx alloys have excellent corrosion resistance.

Compared to another automotive structural extrusion alloy 7xxx, 6xxx alloys are more suitable for complicated and thinner cross-sections. The mechanical properties of both 7xxx and 6xxx alloys are given in Table 1. Besides the higher strength values of 7xxx, not have enough corrosion resistance as 6xxx. Except 7004 and 7005, 7xxx series of aluminum alloys are not suitable for welding. [5]

Table 1: Mechanical properties of 6xxx and 7xxx aluminum alloys [5]

Alloy	Ultimate Tensile Strength (MPa)	Tensile Yield Strength (MPa)	Elongation (%)	Ultimate Shear Strength (MPa)	Modulus of Elasticity (GPa)
6005 T5	305	270	12	200	69
6061 T1	150	90	20	100	69
6061 T4	240	145	22	165	69
6061 T6	310	275	12	205	69
6063 T4	170	90	22	105	69
6063 T5	185	145	12	115	69
6063 T6	240	215	12	150	69
7004 T5	400	340	15	220	72
7005 T53	395	350	15	225	72
7116 T5	360	315	14	200	70
7029 T5	430	380	15	270	70
7129 T5	430	380	14	270	70

For aluminum space frame members, 6063 aluminum alloy is most common selection because of its extrubility, crash energy absorption and excellent mechanical properties after aging. Besides automotive industry, it is also chosen in structure and architecture industry and in electronical and mechanical parts. Microstructure of typical 6063 alloy consists of αAlFeSi, Mg_2Si precipitates and other impurities. These Mg_2Si particles are so fine that cannot be seen with a light microscope, only

visible in electron microscope. 6063 alloy contains approximately 1% Mg_2Si in the structure. [13, 24]

2.3.2 Moment of Inertia

Moment of inertia is a property of physics of an object that is indicated by a force to set any object in motion with a respect to an axis. In other words, moment of inertia determines the ability of deflection of an object. Moment becomes minimum when the axis passes through the center of gravity.

It is defined by I and calculated by using the equation;

$$I = mr^2$$
<div align="right">Eq.1</div>

I = Moment of Inertia (kg m^2), m = Mass (kg), radius (m)

Another equation for rectangular cross-sections is shown below;

$$I = b.h^3 / 12$$
<div align="right">Eq.2</div>

Polar Moment of Inertia is a measure of resistance to rotational acceleration so it shows how difficult to rotate an object on an axis. While the mass is far from the axis of rotation, it is harder to make it turn and object have a high polar moment of inertia. [13]

In automobile, it is important to calculate the polar moment of inertia and center of gravity terms. When the center of gravity of a car is between two wheels, it leads lower polar moment of inertia and which gives higher resistance against torsional forces during turning from corners.

In aluminum structure designing, moment of inertia and modulus of elasticity are important properties in determining equivalent stiffness as steel. Thickness of aluminum parts need to be increased to provide same stiffness and same deflections under bending loads. Even increasing in thickness, aluminum is still lighter than steel at about 44%. In some cases changing cross-section shapes, according to moment of inertia results, are more advantageous rather than increasing thickness. Comparison

of rectangular bars according to cross - sections changes and effect on weight is shown in Figure 4. The three cross – sections with a different weight and moment of inertia have equal stiffness. [6]

	Carbon steel	Aluminum alloy	Magnesium alloy
Specific weight	7.85	2.7	1.75
Modulus of Elasticity "E", MPa	210 000	70 000	46 000
Height "h" for the section with equal base dimension "a"	100	144	166
(The arrows indicate the direction of load.)			
P = Weight	100	50	37
I = Moment of inertia	1	3.0	4.7

Figure 4: Comparison of moment of inertia for different alloys with changing rectangular cross – sections and effect on weight [13]

2.4 Heat Treatment

Aluminum heat treatment takes place in three steps; solutionizing, quenching and aging. Solutionizing temperature and time, cooling rate and aging temperature and time are important parameters for aluminum wrought and casting alloys.

2.4.1 Solutionizing

The purpose of this step is to obtain solutinizing in single phase. In the beginning, microstructure consists of non-equilibrium phase of β and α. Then alloy is heated up above the solidus temperature and β phase is dissolved in α phase. This process continues until all structure becomes a homogeneous phase. Solutionizing temperature must be chosen under melting temperature. If the alloy stays above solidus temperature for a long time as overheating, reducing in mechanical properties such as tensile strength, ductility and fracture is occured. [25]

After solutinizing a single phase is formed at solidus temperature and then quenching is occurred rapidly to obtain supersaturated solution at room temperature. Microstructure forms significantly and be ready for precipitation hardening. If metal is left to cool slowly, β phase starts to nuclei heterogeneously and form equilibrium α+β phase. According to the thickness, quenching temperature changes from room temperature to the boiling point to prevent any distortion. For thinner parts, temperature increases to 65 ºC or 80 ºC to get advantage of cooling rate with reducing internal stresses. [11, 25]

2.4.2 Aging

After quenching process, precipitation hardening can be obtained at room temperature (natural aging) or above room temperature (artificial aging) with increasing diffusion rate. Only difference is the diffusion rate that is provided from heating.

During diffusion in artificial aging process, B atoms form regional concentrations on specific planes in lattice A which is called GP (Guinier – Preston) zones. Then GP zones create nucleation sites to form coherent intermediate phases and these phases deform the matrix to progress and settlement in structure. Movement of atoms is occurred in short distances and finely dispersed in the matrix. [15]

In heat treating aluminum alloys, there are different selections of aging procedure for each alloy. T6 is most widely used heat treatment for casting alloys that contains solutinizing and artificial aging. Mg_2Si is begun to precipitate at 135 ºC and above this temperature Mg_2Si becomes lamellar. At 482 ºC, Mg_2Si is totally dissolved in matrix and alloy is cooled rapidly. In quench process, there is a risk of porosity because of expansion of gas bubbles in part and close to the surface at elevated temperature. After rapid cooling, alloy is heated up to 180 ºC and kept in this temperature for 6 hours to achieve desired mechanical properties. Precipitation mechanism occurs in small scale that cannot examine in light microscopy, so X-rays and electron microscope is needed. [12, 24]

Extrusion alloys (e.g. 6063) are cooled from elevated temperature and artificially aged which is called T5. Solutinizing process is occurred after extrusion process with rapid cooling onto hot profile. There is 1% Mg_2Si in 6063 aluminum alloy and Mg_2Si is soluble approximately in 500 ºC. After rapid cooling, this supersaturated solution is heated up below 204 ºC and kept in that temperature for a specific time to obtain precipitation hardening at microscopic scale. Typical 6063-T5 contains αAlFeSi and Mg_2Si precipitations in microstructure. [24]

2.4.3 Annealing

Solutinizing and quenching may not be suitable for all complex larger parts because of the risk of deformation. In this reason, annealing heat treatment (symbolized as "O") is done to achieve more ductile material with increasing elongation and relieving stress. There is no change in strength when annealing heat treatment is done. Material is subjected to a heating at a temperature between 315 – 345 ºC. For Silafont – 36 alloy, this treatment is done at 320 ºC for 30 – 60 minutes. [26]

2.5 Exposed Loads on Chassis

In addition to being important design criteria of cost, production method and volume, the most critical factor for chassis is to maintain the overall shape against exposed loads. When designing an aluminum chassis, it is important to take into account structural dynamics, static stiffness, crash performance and weight optimization. An automobile is subjected many loads and vibrations internally and externally. Parking car is exposed dead loads (self-weight of structure) constantly and must sustain its structural performance which is related to its stiffness and strength. On the other hand, live load (e.g. vibrations, impact, moment, fatigue) effects on structures in short periods which should not be ignored. [27] When designing a structure, safety factor is determined as 1.1 for dead loads and 1.5 for live loads. [6]

2.5.1. Static Loads

Prior to movement of the vehicle, chassis must be a solid structure against loads (engine, luggage and passengers weight) and meet the forces that are transmitted from suspension. In this reason, stiffness is the major property for structures which is desired as high as possible and described with two parameters; bending and torsional stiffness. With a high stiffness, handling and vibration characteristics are improved. During the design, cost and weight are also considered to achieve a sufficient rigidity. [28]

Bending stiffness of a structure shows the vertical deflection resistance between two wheels as a result of static loads, Figure 5. A chassis structure must be compensated maximum loads on axis which is located at the center of gravity without any deflection. As a result of this, parts to be used are selected and designed to meet vertical loads. In selection of parts; modulus of elasticity, shape and dimensions of cross-sections should be taken into account. Due to the lower elastic modulus than steel, aluminum chassis can meet the same loads with increasing moment of inertia, especially by changing height and length. [29]
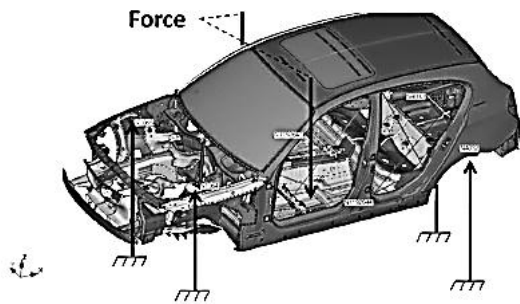
Figure 5: The schematically view of bending stiffness analysis [30]

Torsional stiffness gives the longitudinal deflection degree as a result of a torque between two wheels. In addition to a being static, it can also be dynamic due to the torque when a single wheel fall into the pit or passes through mound and other wheels reacts differently at the same time. Torsional stiffness is determined with applying forces in opposite directions to the chassis which is shown in Figure 6. (35)

Space frame type of chassis shows high roll stiffness and becomes higher with the number of frames increases but weight should be kept in view. High stiffness also increases handling performances otherwise poor handling may cause fatigue by the effect of rotation on the chassis and result a failure in a short period.
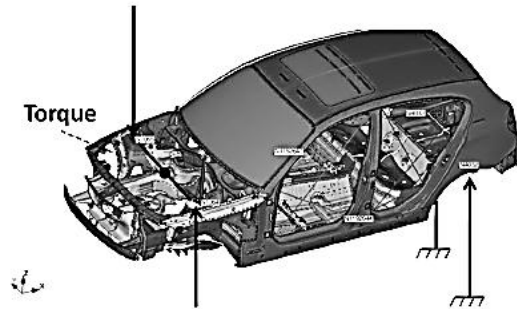
Figure 6: The schematically view of torsional stiffness analysis [30]

2.5.2 Dynamic Loads

Besides the structural rigidity, chassis is in motion must also protect these features. On the other hand, chassis need to hinder any failure against different forces in difficult road conditions and must show sufficient safety during impacts. Frames are exposed to bending, torsion and folding loads during the crash. In this case, due to the difficult and expensive to determine the loads from the road, finite element method is more accurate for dynamic analysis.

Passenger safety is an important issue in car accidents so front, rare and side parts are designed to satisfy enough mechanical properties to avoid any fatal situation. Priority to avoid collapse during crash, passenger cell must be in sufficient rigidity. In addition, materials and cross-sections are selected in order to absorb enough energy without transmitting it to the passengers. [31]

Side impacts are dangerous for occupants because there is not enough space to prevent kinetic energy. In this reason, frames that make up the passenger cell must maintain the structural stiffness when vertical and diagonal forces are applied. At this

19

point, B - pillar becomes so important and should be strong enough to prevent these forces. Also doors are strengthened to support B – pillar but when the doors become larger, it becomes difficult to support with losing their stiffness. [27]

Front parts that are subjected to impact during crash are very important and providing safety of passengers with collapsing. For substantial collapse characteristics, design should be suitable to overcome with minimum passenger injury. There are many studies have been done about determining the cross-sections and frames shapes for frontal parts and S-shaped frames shows significant energy absorption during crash. [32, 33] Energy-absorbing components should be selected carefully. If the material has a high deformation property with a low strength, collapse becomes higher and deformation will be occurred in passenger cell which may cause a fatal injury. If low deformation and high strength is selected (e.g. steel), energy is transmitted directly to the passengers with sudden deceleration and it causes problems on safety. [27]

Energy absorption which has a vital importance for passengers during crash is required to ensure maximum safety. Materials are selected carefully according to their energy absorption capacity. For this reason, aluminum is widely used in frontal impact parts with their high energy absorption properties. The critical factor in energy absorption is the stress – strain characteristics and determining with the area under the curve. But in the cases with the dynamic property, strain rate sensitivity becomes more important during the crash because of non-linear loads. Materials with high strain rate sensitivity, absorbs more energy. These types of collisions with high strain rate are obtained with finite element modeling accurately. In the NCAP (New Car Assessment Program) Standard, crash speed is assumed as 64 km/h which is the maximum speed for fatal injuries during the collision as a passenger [27, 28]

2.5.3 Fatigue

Materials that are subjected to dynamic loads undergo progressive and local structure damage. If the loads are above the specific level, microscopic cracks start to occur on material surface. In time these cracks will reach a critical size and failure in structure

occurs. The shape of the structure is affected the fatigue life significantly. Stress range and number of cycles are also effected the fatigue strength.

Fatigue life of material is determined with number of cycles of loads that are assisted to form cracks and growing until critical size. In a classical way, fatigue life is obtained from S-N curves. (S: stress range, N: number of cycle). Curve goes down with increasing cycle. When there is not any failure on material in a specific time is called fatigue endurance limit. [15]

Fatigue characteristics are examined in two categories. Under high stress and short periods (N: $10^4 - 10^5$), low-cycle fatigue, occurs in elastic-plastic deformation area. When it is subjected to low stress and occurs in elastic deformation region is called high-cycle fatigue and gives longer lives results. (N: 10^7) [34]

Fatigue analyses are determined in two loading cases. Constant amplitude with proportional loading is the simple failure calculation that maximum and minimum loads applied to parts stay constant in a specific period. After load is applied, same and opposite load is applied again and load ratio is defined as -1. On the other hand constant amplitude with non-proportional loading is used when two loading is applied in same points. So that two conditions like tension and compression or torsion and bending can be evaluated together. In this case, instead of a single ratio, alternating and mean stress are calculated and load ratio varies with time is obtained. For mean stress calculation three methods have been developed; Goodman, Gerber and Soderberg which are shown in Figure 7. While Goodman is a good choice for brittle materials, Gerber is suitable for ductile materials and Soderberg is used generally for low ductility materials. The Gerber theory also treats negative and positive mean stresses the same. [35]
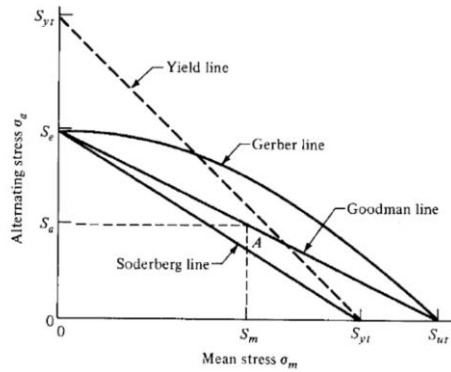
Figure 7: The mean stress curves of Soderberg, Goodman and Gerber [35]

2.6 Welding

Aluminum welding is most widely used joining process in space frame technology. Compared to steel, some of the features that are unique to the material should be considered when welding aluminum materials. Aluminum has higher electrical conductivity than steel so cannot show enough resistance in spot welding to provide joint, in this reason fusion welding is more preferred for aluminum. [1] On the other hand with a higher thermal conductivity of aluminum, removal of gases from welding pool is also delayed. As a result, insufficient melting and pores in weld seam may occur. In order to prevent this, first step must be to clean the welding region before welding.

In addition, annealing thicker parts and preheating can prevent this kind of welding failure. Preheating besides reducing stress of solidified metal, provides faster joining rate and should be done at a temperature between 205 – 425 ℃. [36] Soluble H_2 diffusion that causes porosity into welding pool is also blocked with preheating. Excess heating results reducing in mechanical properties of parent metal, for this reason preheating should be done carefully in heat treatable aluminum alloys. [37]

Aluminum alloys with higher fluidity shows better welding properties. When low solid solubility elements as Si are included in aluminum alloys, dispersed Al-Si small areas are formed after welding. [38] Also sharp and brittle phases should be

considered because large heterogeneous areas reduce fatigue strength. For this reason after welding, parts need to be subjected to heat treatment. But heat treatment of large-scale parts after welding is mostly not practical; therefore heat treatment before welding is also beneficial.

When HAZ (Heat Affected Zone) is examined in precipitation hardened Al-Si-Mg alloys (6xxx series) after welding, decreasing in hardness is observed in that zone because of dissolution of precipitates. HAZ in 6xxx aluminum alloys has lower hardness compared to welding metal which is shown in Figure 8. This region becomes approximately 30 mm with a temperature at 100 ºC in TIG welding process. [39]
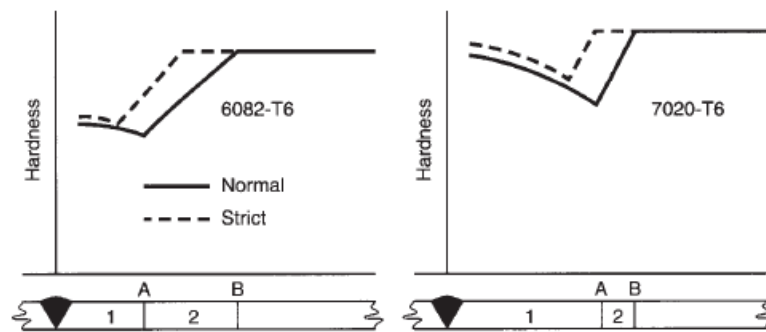
Figure 8: Hardness curve at a weld in 6xxx and 7xxx aluminum alloys [39]

In TIG (Tungsten Inert Gas) welding, welding arc occurs between work piece and tungsten electrode and at the same time filler metal is added to the welding pool. Ease of use from different angles and compatibility of any joint types are the factors that TIG welding is preferred process for aluminum. Also the welding can easily be checked during process and thinner parts can be welded with changing current. [36] Argon is used as an inert gas to protect welding region from diffusion of H_2 and with help of the slow cooling, porosity is prevented. Two different methods (AC and DC) are used in TIG welding and AC type is more preferred when thinner parts are need to be welded. [40]

Selection of filler metal is an important criterion in TIG welding. Proper filler metal selection creates a big impact on the service life of welding. Preferred filler metals

for aluminum alloys and their contents are shown in Table 2. 4043 alloy is developed especially for 6xxx series and heat treatable alloys welding. High Mg in aluminum alloys and Si from filler metal form Mg_2Si and this reduce ductility, due to this reason 4043 alloy as a filler metal is not preferred in high Mg contents above 3%. [38] Due to low melting point of 4043, wetting of metal becomes better and tendency of hot crack formation is reduced in parent metal at 6xxx series with its high fluidity. So that shrinkage spaces are fed easily. Despite higher strength and ductility is provided with using 5356 filler metal, problems are observed because of insufficient penetration. In this reason, due to good penetration and sufficient mechanical properties 4043 filler metal is more preferred. [13, 36, 39]

Table 2: The composition of filler metals for aluminum alloys [41]

Alloy	Si	Fe	Cu	Mn	Mg	Cr	Zn	Ti
1100	b	b	0.05 - 0.20	0.05	-	-	0.10	-
2319	0.2	0.03	5.8 - 6.8	0.20 - 0.40	0.02	-	0.10	0.10 - 0.20
4043	4.5 - 6.0	0.8	0.3	0.05	0.05	-	0.10	0.20
4047	11.0 - 13.0	0.8	0.3	0.15	0.10	-	0.20	-
4145	9.3 - 10.7	0.8	3.3 - 4.7	0.15	0.15	0.15	0.20	-
4643	3.6 - 4.6	0.8	0.1	0.05	0.10 - 0.30	-	0.10	0.15
5183	0.4	0.4	0.1	0.50 - 1.00	4.3 - 5.2	0.05 - 0.25	0.25	0.15
5356	0.25	0.4	0.1	0.05 - 0.20	4.5 - 5.5	0.05 - 0.20	0.10	0.06 - 0.20
5554	0.25	0.4	0.1	0.50 - 1.00	2.4 - 3.0	0.05 - 0.20	0.25	0.05 - 0.20
5556	0.25	0.4	0.1	0.50 - 1.00	4.7 - 5.5	0.05 - 0.20	0.25	0.05 - 0.20

Hot cracking is usually seen in heat treatable alloys and occurs during cooling in welding under extreme stresses. All cracks during welding are called as hot cracks. The most important way to prevent hot cracking is to select proper joint design and filler metal. [37, 40] With selection of butt joint type, more parent metal is taken into melt and dilutes the filler metal and due to this dilution hot cracking tendency is reduced. In addition, welding occurs in butt joint design shows longer fatigue life under dynamic load with high strength. The wide range of solidification is the most important reason for the hot cracking formation, from there pure and eutectic alloys show less tendency to hot cracking. Because solidification is occurred at constant temperature in eutectic alloys and they are exposed less stresses.

2.7 Stress Corrosion Cracking

Stress corrosion cracking is a fracture of material under corrosion with a static tensile stresses that are formed by external loads or residual stresses. In this form of corrosion, resistance is reduced with creating cracks in the material. Fracture occurs by the stress corrosion cracking is usually sudden and not predictable. So the material which is placed in corrosive environment under tension of sufficient magnitude will fail in lower stresses than expected. Process is undergoing in three steps respectively; crack initiation, crack propagation and fracture. [56]

Aluminum alloys that are containing large amounts of alloying elements such as copper, magnesium, silicon and zinc cannot show enough resistance against stress corrosion cracking. When the aluminum and alloys are exposed to special environments and sufficiently large forces at the same time, damage occur along the grain boundaries. The characteristic of stress corrosion cracking in aluminum alloys is intergranular. [11, 56]

Generally, high strength aluminum alloys such as 2xxx and 7xxx are susceptible to the stress corrosion cracking. On the other hand, most 5xxx and 6xxx aluminum alloys have a resistance against stress corrosion cracking. But in some cases such as high percentage of copper and excess ratio of the Mg_2Si in 6xxx aluminum alloys become susceptible to the stress corrosion cracking at high stresses and in aggressive solution. Aluminum alloys that are containing more than 3% magnesium in excess of solid solubility limit can become susceptible to stress corrosion cracking. Also 6xxx aluminum alloys that are subjected to solutinizing heat treatment may show some minor susceptibility to intergranular corrosion. In casting alloys, stress corrosion cracking is rarely occurred. 3xx and 4xx aluminum casting alloys are resistant against stress corrosion cracking, but again the alloys which contains copper show lower resistance. Silicon effects minimum to the resistance of corrosion in casting alloys. But impurities such as copper, lead, nickel and iron may be harmful even in small volumes. [7, 11] Consequently, 6063 aluminum wrought alloy and Silafont – 36 aluminum casting alloy has no susceptibility to stress corrosion cracking. [12]

CHAPTER 3

EXPERIMENTAL PROCEDURE

The experimental procedure consists of production method and proper alloy selection for each part in aluminum space frame. High toughness and high fluidity were desired while selecting proper aluminum alloy. Then parts were manufactured via sand casting and extrusion processes and subjected to heat treatment in several times and conditions. In order to create a structure with high stiffness, cross-section design of individual parts were obtained according to moment of inertia calculations. Space frame design was analyzed against bending and stiffness loads with using finite element method. On the other hand, fatigue life and safety factor of space frame was also investigated.

3.1 Sand Casting

Sand casting is most feasible method to produce complex shapes for low production volumes with its low cost. In this study space frame pillar parts, shock absorber and support parts for joint areas were produced with using sand casting (silica sand and clay bonder) method. Selection criteria were investigated to choose proper alloy in experiments. Fluidity and mechanical properties are major concerns while choosing sand casting alloy. In our experiments besides sand casting alloys, permanent casting alloys were also considered. According to the theory and experiences of car companies and compatibility of heat treatment, Si based 3xx and 4xx series of aluminum alloys and Silafont-36 (AlSi9Mg) which is a trademark of Rheinfelden

(Germany), were selected. The candidate alloys' compositions, mechanical and physical properties are given in Table 3, 4, 5 respectively.

Table 3: The chemical compositions of candidate alloys for spiral fluidity test [42]

Alloy	Cu	Mg	Mn	Si	Fe	Zn	Ti
A356.0	0.2	0.35	0.1	7.0	0.25	0.1	-
A357.0	-	0.5	-	7.0	-	-	-
B390.0	4.5	0.6	-	17.0	-	0.5	-
A413.2	-	-	-	12.0	2.0	-	-
Silafont-36	0.03	0.35	0.6	10.5	0.15	0.07	0.15

Table 4: The physical properties of candidate alloys for spiral fluidity test [42]

	A356.0 T6 (Sand Cast)	A357.0 T62 (Sand Cast)	B390.0 T6 (Sand Cast)	A413.2 F (Die Cast)	Silafont – 36 T6 (Die Cast)
Melting Range (ºC)	560 - 615	560-615	516 - 582	574 - 582	550 – 590
Density (g/cm^3)	2,68	2,67	2,73	2,66	2,64
Thermal Conductivity (W / (K x m)	151	150	134	121	139 – 168

Table 5: The mechanical properties of candidate alloys for spiral fluidity test [42]

	A356.0 T6 (Sand Cast)	A357.0 T62 (Sand Cast)	B390.0 T6 (Sand Cast)	A413.2 F (Die Cast)	Silafont – 36 T6 (Die Cast)
Tensile Strength (MPa)	230	315	280	290	310
Yield Strength (MPa)	165	250	280	130	245
Elongation (%)	3.5	3.0	<1.0	3.5	8.0
Hardness (HB)	70 - 105	85	80	80	90 -110
Fatigue Resistance (MPa)	70	85	75	71	89
Modulus of Elasticity (GPa)	72,4	73	80	71	70 - 80

3.1.1 Spiral Fluidity Test

Fluidity is an important parameter while producing thinner chassis parts. Metals with the high fluidity fill the mold cavities easily during solidification. Spiral fluidity test is used to determine the castability of alloys with measuring the flow length of the molten metal in spiral cavity, the schematically view is shown in Figure 9.
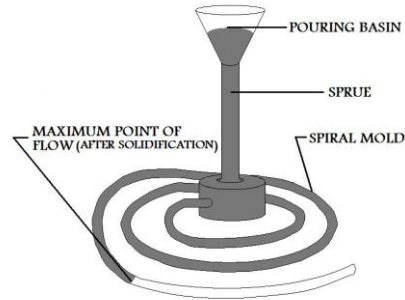
Figure 9: The schematically view of spiral fluidity test [43]

In our experiments, six candidate alloys were melted in induction furnace at 800 ± 5 ºC with the constant mass, 400 gr. When molten metal reached sufficient temperature, Nitrogen degassing process was applied for $10 - 15$ minutes into the furnace to prevent gas porosity. Then molten metal were poured into the spiral sand cavity at a temperature of 750 ± 10 ºC because of a heat loss by transportation approximately $50 - 60$ ºC. After the solidification process was finished, spiral aluminum specimens were taken out of the mold and the maximum flow length was measured and compared.

3.1.2 Mechanical Properties of A356.0 and Silafont – 36

According to the fluidity test, the number of candidate alloys was reduced. A356.0 and Silafont-36 (AlSi9Mg) became most appropriate alloys with their sufficient fluidity and mechanical properties from standards. Due to Silafont – 36 is a die casting alloy, mechanical properties of sand casting are to be determined. For this

reason, tensile test was conducted to make a comparison in mechanical properties between A356.0 and Silafont – 36.

Melting temperature and procedure were selected the same as in spiral fluidity test. For grain refinement, AlTi5B1 master alloy was added to the molten metal as containing 0.15 % Ti in total melt. AlTi5B1 grain refiner includes 5% titanium and 1% boron.

After all AlTiB was molten in the metal, AlSr10 which is the eutectic modifier and contains 10% strontium was also added to molten metal before pouring. Grain refinement and eutectic modification was done to achieve higher mechanical properties for each alloy. Then nitrogen degassing operation has been held and pouring was occurred into the sand mold.

Rods were produced for tensile test as a length of 200 mm and a diameter of 8 mm. These rods were sent to turning machine to obtain standard tensile test specimens. Geometries of specimens used in tensile test are shown in Figure 10. The tensile test was held via Mares TST-RE universal testing machine (see Figure 11) which has a maximum load capacity as 50 tones. Tests were carried out at a speed of 1 mm / min and ended when aluminum specimens failed. Ultimate tensile strength and load – displacement curve were obtained from program.
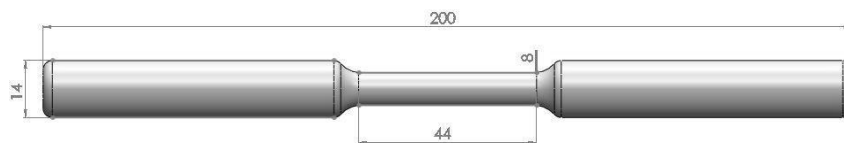
Figure 10: Geometry and dimensions of tensile test sample

Figure 11: Tensile test equipment used in experiments

3.1.3 Mechanical Properties Change with Heat Treatment

The mechanical properties are varied by heat treatment therefore precipitation hardening needs to be done to improve mechanical properties. Again Silafont − 36 is a permanent casting alloy; mechanical properties after heat treatment were unknown. In this experiment, sand cast Silafont − 36 alloy was subjected to heat treatment at different temperatures and times to obtain the desired mechanical properties.

In order to develop a similar composition of Silafont − 36, primer aluminum was selected with low iron content called ETIAL - 9 from Eti Aluminum (see Table 6). Other additional elements were added into the melting and blending. After grain refinement and eutectic modification were done, spectrometer analysis was taken.

Table 6: The chemical compositions of primer aluminum that was used in sand casting [44]

	Al	Fe	Si	Cu	Zn	Ti	Mn
ETIAL - 8	99,8	0,15	0,1	0,03	0,03	0,02	0,02

For determining the grain refinement and modification effect, thermal analyses were carried out. Molten aluminum at 750 ºC was poured into square thermal analysis cups and temperature change was read from Elimko 680 universal thermal analysis device. Thermal analyses were taken place for 10 minutes and instant temperature for each second was collected. First derivative of data were derived in MatLab R2012a, curves were drawn to find elapsed time and eutectic solidification temperature of each phase. Also liquidus and eutectic undercooling were determined.

In addition to this, samples for microanalysis were taken before and after modification to determine the modification results. The samples were grinded from 80 to 1200 grit SiC paper by water cooling. Then polishing was done with 3 and 1 micron Al_2O_3 abrasive. After polishing, specimens were etched in Keller etchant (1% HF, 1.5% HCl, 2.5% HNO3, 95% H2O). Olympus optical light microscope was used to investigate the microstructure of the specimens. Images were taken at 100x and 200x magnification

Grain refined and eutectic modified Silafont – 36 alloy was melted in induction furnace and 20 x 35 mm small square specimens for hardness test were produced via sand casting. For solutionizing process, temperature was selected at 490 ºC which is the minimum soluble temperature of Mg_2Si in aluminum alloy including Si between 9.5 – 11.5%. Different solutionizing times (2, 3 and 4 hours) were carried out at this temperature in resistance furnace and then hot quench was done at 60 ºC. Hot quench was occurred to prevent any distortion while quenching thinner parts. After solutionizing, samples were subjected to artificial aging at 170 ºC between 4 – 7 hours.

Investigating the hardness change by heat treatment, specimens were subjected to Brinell Hardness Test on the basis of the standards of ASTM E10-12. [45] The test was carried on at 62.5 kg load by steel ball with a diameter of 5 mm via EMCO Test M4U-C25 universal test machine. (see Figure 12) Values from the hardness test were placed on the table by taking the arithmetic mean and curve was drawn.

For complex large parts of chassis, annealing was carried out in heat treatment furnace under controlled atmosphere. According to the similar composition of

Silafont – 36, parts were heated up to 320 ºC for 60 minutes. After annealing heat treatment, parts were subjected to the tensile test to obtain changing in ductility.

Figure 12: Hardness test machine used in experiments

Tensile tests were held in Mares TST-RE universal test machine. Fabricated, annealed and heat treated samples (see Table 7) were applied to tensile test to observe the changing in ultimate tensile strength and elongation. Tests were carried out with 1 mm / min strain rate and ended when specimens failed. Data was collected from program and change in mechanical properties with various heat treatments were shown in graph.

Table 7: Tensile test sample process for each heat-treatment (*T6 Heat Treatment was done as a next step of T4 heat treatment for aging process)

Treatment Type	Temperature (ºC)	Time (Hour)
Fabricated (Untreated)	-	-
Annealed	320	1
Heat Treatment (T4)	490	3
Heat Treatment (T6)*	170	6

In order to investigate the impact behavior and energy absorbance of different treated cast parts against dynamic impacts, Charpy impact test was done at the same conditions as tensile test. Charpy impact tests were held at room temperature by Tinius Olsen 358 joule testing machine according to basis of the standards of ASTM E – 23. [46] The dimensions of test samples and Charpy impact test equipment are shown in Figure 13.
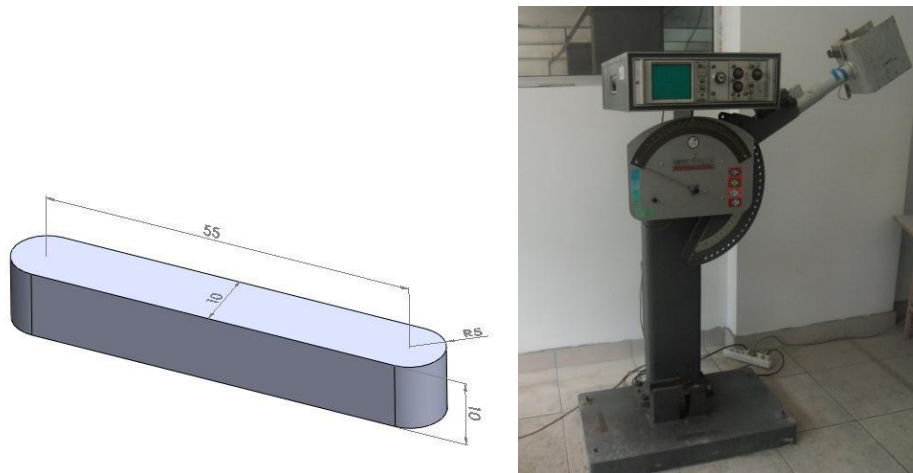
Figure 13: (left) Geometry and dimensions of Charpy impact test sample, (right) Charpy impact test machine used in experiments

3.2 Extrusion

3.2.1 Hardness – Heat Treatment Curve

For aluminum extrusion samples, artificial aging process was carried out at 185 ºC for several hours. The phase diagram of Al – Si with respect to Mg_2Si ratio, as a composition of 6063 aluminum alloy, is shown in Figure 14. 6063 aluminum alloys as a nominal composition, is included 1% Mg_2Si and from this Mg_2Si melts at 500 ºC in aluminum. Because of aluminum profiles were subjected to cooling process after leaving the die, solutionizing was no more needed and profiles were ready to aging process. Against other possibilities, some extrusion samples were also taken into

solution and quench at room temperature. ASTM B918/B918M-09 Standards [47] was used to determine temperature and time as 520 ºC and 8 hours respectively for solutinizing.

Samples were divided into two categories as T6 and T5 heat treatment and heated up to 185 ºC and 205 ºC respectively in resistance furnace for artificial aging. In these temperatures, specimens were held in different times. At 185 ºC, samples were held between 2 to 20 hours and at 200 ºC for 1 -3 hours. Then all samples were removed from furnace respectively and left in room temperature for 24 hours. All samples were tested by Brinell hardness was taken by EMCO Test M4U-C25 universal test machine with a 2, 5 mm steel ball indenter under 187, 5 kg load. The hardness – heat treatment curve was generated with the obtained hardness values.
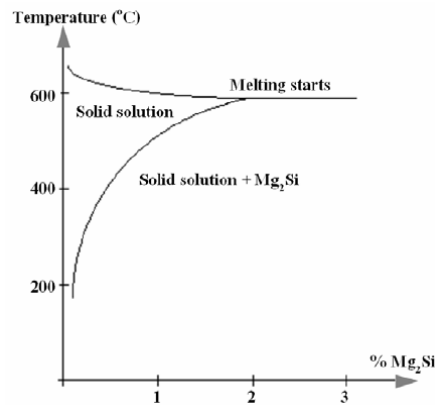
Figure 14: Phase diagram of 6063 aluminum alloy for solution heat-treatment [48]

3.2.2 Three Point Bending Test

Three point bending test was done to examine deformation characteristic and energy absorbance of aluminum extrusion profiles under compressive loads. Also experiments under static loads may help to reveal dynamic influence on them. In order to maintain these results three specimen were selected; untreated and heat-treated aluminum extrusion profiles (6063) and square steel profile (AISI 1015). Dimensions and mechanical properties of these profiles are given at Table 8 and 9 respectively. Tests were performed according to the basis of standards of ASTM

E290 - 09 [50] by Mares TST-RE tensile test machine at room temperature with a 1 mm/min strain rate. Profiles were fixed with two supports and cylindrical intender was set up to the center point of profile. Intender diameter was 15 mm and distance between two plungers was set up as 350 mm. Maximum displacements was set to 80 mm and tests were ended when profiles failed. Load – displacement data were read from computer screen and curve was drawn with giving values. Energy absorption was calculated from the area under the curve and all results were compared. Surface cracks and fractures after flexural test were also investigated.

Table 8: The dimensions of profiles that were subjected to the 3-point bending test

Specimen	Length (mm)	Height (mm)	Width (mm)
6063 - T4	300	50	80
6063 – T6	300	50	80
Carbon Steel	300	50	50

Table 9: The mechanical properties of alloys that were subjected to the 3-point bending test

Alloy	Ultimate Tensile Strength (MPa)	Yield Strength (MPa)	Elongation (%)
6063 – T4	172	89	22
6063 – T6	241	214	12
Carbon Steel	385	325	18

3.2.3 Moments of Inertia of Different Cross Sections

When steel chassis was revised to the aluminum, it is important to compensate same mechanical properties. Besides selecting the proper alloy, design is also a major factor while working under loads. In this reason, cross – section must be changed to maintain sufficient properties as steel under a safety area. Moment of inertia calculations were done to figure out the comparison as theoretically and extrusion profiles were produced according to results.
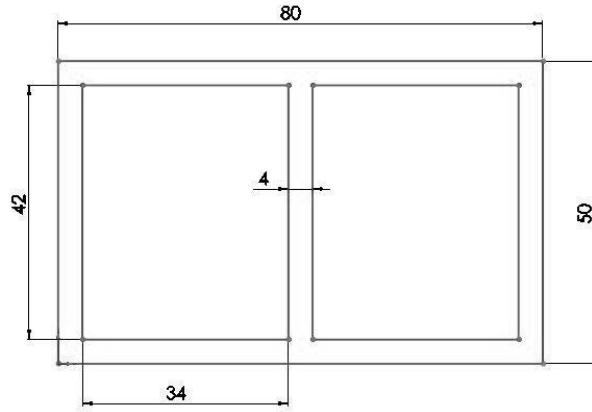
Figure 15: Cross – section geometry and dimensions of aluminum profile

Aluminum profile's cross-section that was used instead of steel on chassis is given on Figure 15. Moment of inertia was calculated from the equation 3 which is used for rectangular cross – sections with giving dimensions.

$$I = \frac{1}{12} b. h^3 \qquad \text{Eq.3}$$

In order to calculate the ultimate and yield strength values from the results of moment of inertia, equation 4 was used. Loads were taken from the load – displacement curve by the results of the experiments in three point bending tests. The possibility of shear stress was also considered and another calculation was done to obtain changing in yield strength.

$$\delta = \frac{M.c}{I} \qquad \text{Eq.4}$$

where δ is bending stress, M is bending moment, c is the dimension from the centroid of the cross section, I is moment of inertia of the cross section.

Same calculation was done for steel profile with the dimensions which are given in Figure 16. Ultimate and tensile strength results were obtained and all results were compared with aluminum profile.
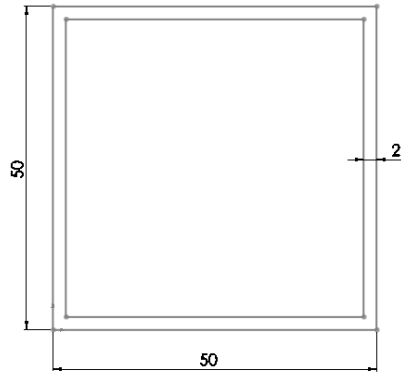
Figure 16: Cross – section geometry and dimensions of steel profile

3.3 Mechanical Properties Variation of Welded Samples

Welding process was done via TIG welding method by Miller Syncrowave 350 LX welding machine (see Figure 17). Welding was carried out at approximately 200 Ampere and between 15-18 Volts in DC method. 4043 filler metal was selecting for welding and argon was used as an inert gas during process.

Figure 17: Welding machine used in experiments

Heat affected zone is an important region for materials that are subjected to welding. In this reason, some experiments were carried out to evaluate the hardness and tensile strength of these regions. Samples were divided into two categories as heat treated and fabricated. Heat-treated samples were subjected to artificial aging process at 185 ºC for 6 hours according to the results of hardness – heat treatment curve experiment. For sand cast samples, solutinizing were occurred at 490°C for 3 hours and artificial aging was done at 170°C for 6 hours. The dimensions of samples were 50 x 150 mm and 5 mm thickness with a plate shape. Two plate samples were welded with each other and hardness tests were observed.

For welded samples, Brinell hardness was taken perpendicular to the welding direction as a distance between 0.5 - 30 mm with increased spacing. Decreasing in hardness at HAZ was investigated and compared with fabricated samples. Hardness results of heat treatment after welding was also observed. In addition to this, hardness was taken in certain time intervals (after 1 and 3 months) from the heat treated and welded profiles to determine the changes with natural aging.

On the other hand observing the mechanical properties of weld seam, tensile test samples were taken perpendicular to the welding. Plates that were cut from extrusion profiles (6063) with a dimension of 80 x 150 and sand cast plates (Silafont – 36) with the same dimensions were prepared. Artificial aging heat treatment was done before welding. Then 4 samples for each extrusion – extrusion and extrusion-sand cast plates were welded together. The basis of standards of EN 895 [49] was taken as reference for tensile test specimens and samples geometry and the dimensions are shown in Figure 18. Weld seam was grinded and 16 tensile test samples with a 4 mm thickness were obtained by spline. Tensile tests were held by Instron 5582 universal testing machine which has a load range between 2 – 100 kN. Tests were carried out with a 1 mm/min strain rate. Ultimate tensile strength was taken from program and the fracture area was investigated.

Micro investigations (EDX and light microscopy) were held to focus on silicon content and microstructure change after welding between extruded and sand cast sample. EDX analysis was carried out by FEI Nova NanoSEM 430 scanning electron microscopy and line scans were done.
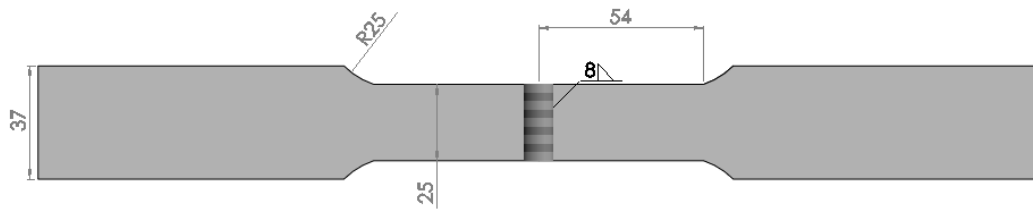
Figure 18: Geometry and dimensions of tensile test samples that were taken from weld seam of two extrusion and sand cast plates

3.4 Finite Element Analysis

Finite Element Analyses were done in this study to investigate the chassis behaviors under static and dynamic loads. Also fatigue properties of joint regions and single parts were determined. It is important to figure out the limits of chassis to maintain driving loads with sufficient mechanical properties and obtain critical areas on design. But some of these results cannot be measured in laboratory areas because of time and cost limitations.

In this reason, Finite Element Method (FEM) is used to determine these measurements via using a mathematical model according to the help of numerical solutions simulation. With using FEM, solutions can be obtained with an acceptable approach to the real physical problems. Models that are represented the real situation are divided into a finite number of elements. These elements are connected to each other at certain points that are called nodes. FEM is attempted to solve the displacements of these nodes according to initial and boundary conditions. Conditions defined for nodes are translated into linear equations, then all these equations are solved and the actual stresses in members are tried to find with finite element method.

In this study, the bending and torsional stiffness of chassis were simulated with static analyses. On the other hand some individual casting parts were analyzed to obtain durability under maximum load. According to stiffness analyses, fatigue characters

of chassis were also simulated. Fatigue life, fatigue damage and safety factor results were obtained. Weak regions were strengthened with respect to fatigue results and maximum stiffness was achieved. In addition to the static engineering problems, dynamic analyses were carried out via dynamic explicit solvers to obtain impact energy absorption and peak force.

ANSYS 13 - Workbench was used for simulation of analyses in this study. For static and fatigue analyses Static Module was selected and for dynamic engineering problems Explicit Module was used. Pre-processing of analyses was done via using ANSYS 13 – Workbench and geometries were designed and extracted from Solidworks 2011 and CATIA V20. CAD parts, material models, meshing parameters, initial and boundary conditions, supports and forces that were applied on parts and other analysis settings were set on program interface. Simulation was carried out with ANSYS – AUTODYN which gives the most intimate and accurate solutions.

3.4.1 Material Models and Analysis Settings for Static Analyses

For stiffness simulations of chassis, some material models were added into engineering data of ANSYS 13 – Workbench. Alloys which were used in analyses were defined such as 6063 – T6 and Silafont – 36. Elasticity and alternating stress R-ratio were also defined to investigate stress distribution at a constant time and according to fatigue life. Decreasing alternating stress changing with respect to the increasing cycle for R-Ratio -1 was written from standards [55] (see Table 10) and S-N curves were drawn for both alloys which are shown in Figure 19. (S is the plot of stress and N is the number of cycles to failure.)

Table 10: The alternating stress at each cycle for 6063 and Silafont – 36 aluminum alloy that were used in finite element analysis

Cycles	Alternating Stress (MPa)	
	6063 – T6	Silafont – 36
10^5	162	193
10^6	114	131
10^7	93	101
10^8	76	84
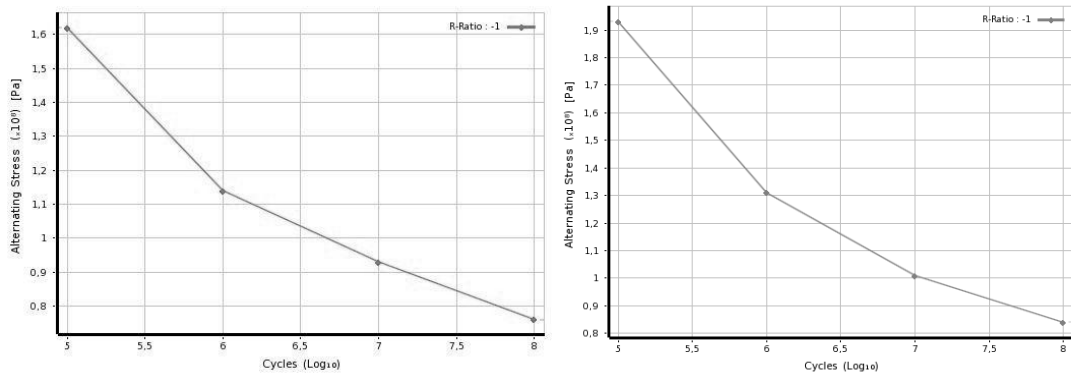
Figure 19: S-N curves of 6063 (left) and Silafont – 36 (right) aluminum alloys

After material data was applied to the parts, meshing was done under a maximum element sizing which is about 1.0×10^{-4}m with hybrid meshing method. For bending analysis, chassis was fixed from four wheels and the estimated total car weight was added to the midpoint in longitudinal direction between two wheels (see Figure 20). Approximately 2000 kg with passengers' weight was applied to the midpoint and deflection of beams was investigated.
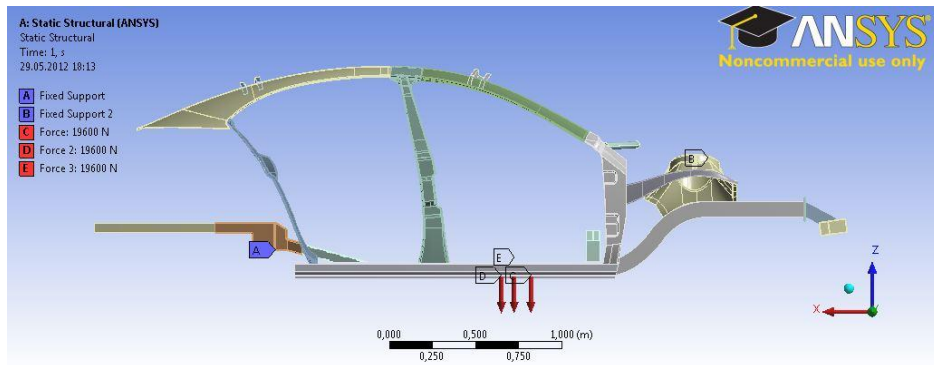
Figure 20: Applied forces and fixing points for bending stiffness analysis captured from ANSYS 13/Static Structural Workbench GUI

Torsional stiffness simulations were handled in two categories; the first chassis was fixed from three points and force was applied from shock absorber and latter moments were given to the shock absorber towers to perform torque movements as boundary conditions to determine the deflection of beams and stress distribution of joint parts. (Figure 21)
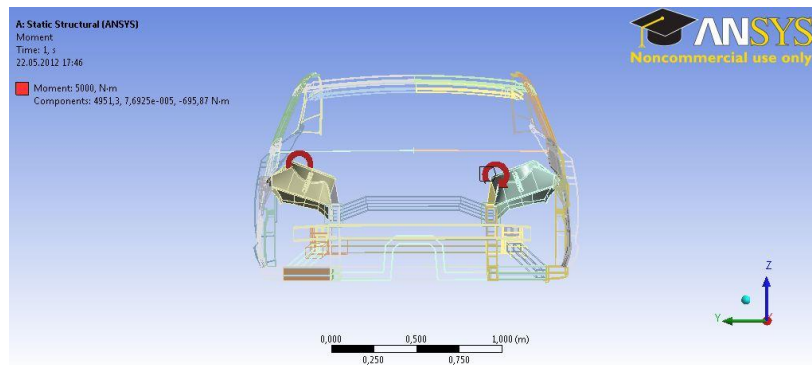
Figure 21: Applied moments for torsional stiffness analysis captured from ANSYS 13/Static Structural Workbench GUI

Torsional stiffness was calculated with the equation 5 and moment over deflection was transferred to the chart. In equation 5, T is the vertical force that was applied to the mounting locations, θ is the deflection and K is the torsional stiffness. Deflection degree is found by using the equation 6 where δ is the amount of vertical deflection of right and left, L is the length between two points.

$$K = \frac{T}{\theta} \qquad\qquad Eq.5$$

$$\theta = \tan^{-1}\left(\frac{|\delta_r| + |\delta_l|}{L}\right) \qquad\qquad Eq.6$$

In addition to the static results of parking car, analyses were carried out under higher loads as an assumption for dynamic loads. Some individual casting parts such as shock absorber, B-pillar and rare joint part were analyzed to obtain maximum load capacity. Parts were fixed from their chassis connection point and load was applied as close to the reality. Analyses were done at 500 kg and 1000 kg loads which are relatively sufficient for individual parts because the rigidity will be increased by assembling. The analysis of rare joint parts was carried out in two methods. First equivalent loads were applied to mounting locations. Second, while 500 kg load was given to the mounting location in rare joint part, 1000 kg was given to another to investigate the deformation and stiffness. Efficiency was calculated and comparison was done after strengthening joint parts with casting.

Fatigue analyses were carried out in two categories; constant amplitude with proportional loading and constant amplitude with non-proportional loading. In constant amplitude load, simulation was held in fully reversed, which means zero mean stress, by S-N curves and fatigue life; damage and safety factor results were obtained. Fully reversed loading is used to apply equivalent and opposite loads which is shown in Figure 22.
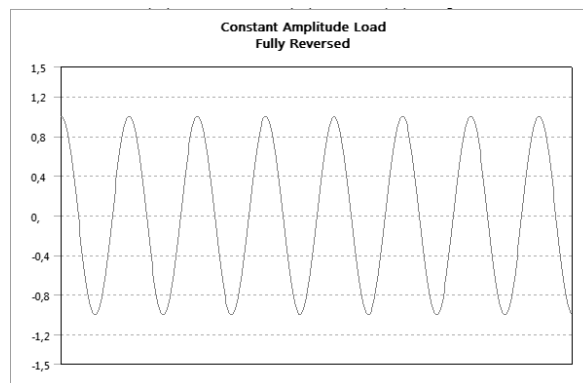
Figure 22: Fully reversed proportional loading of constant amplitude fatigue analysis captured from ANSYS 13 Fatigue Tool

In constant amplitude with non-proportional loading analysis, while stress amplitude is not changing over time, applied load is not constant and change between two loads. In automobile, loading is never subjected constantly so this analysis type is assisted to find closer results to the reality during driving. Two environments were created and changing loads were applied as 500 kg and 1000 kg to the single shock absorber. Solutions were combined and loading type was selected as non-proportional as shown in Figure 24. Gerber was selected as mean stress correction theory. (Figure 23) If the point of the combined stress is below the Gerber line then the component will not fail. Stress distribution and fatigue results were discussed.
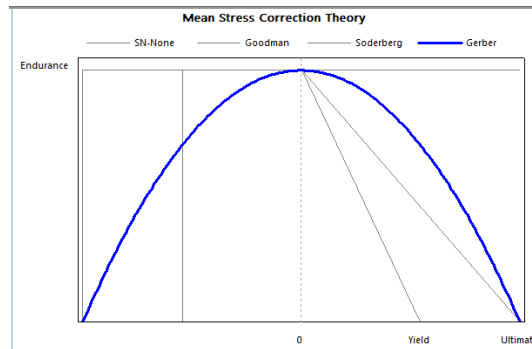
Figure 23: Gerber mean stress curve that were used in fatigue analysis captured from ANSYS 13 Fatigue Tool
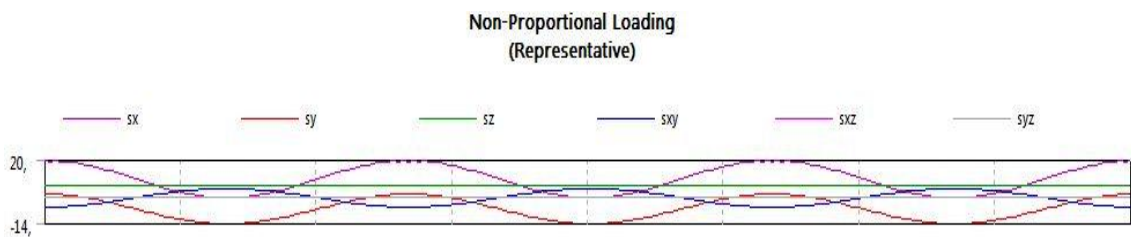
Figure 24: Non-proportional loading curves of constant amplitude fatigue analysis captured from ANSYS 13 Fatigue Tool

3.4.2 Material Models and Analysis Settings for Dynamic Analyses

For dynamic impact analysis of profile, material properties of 6063 – T6 was added into engineering data of ANSYS 13 – Workbench. In addition to elasticity, plasticity was also defined against dynamic conditions. Plastic behavior of material regarding strain rate dependency was defined as Johnson – Cook model. This model is used to determine the dynamic fracture strain of the material influenced by local stress, strain rate and local temperature. During frontal impact of chassis, non-constant strain rate is affected to the material and yield strength is changing according to it. The formula of model is shown in equation 7 [51] where δ_Y is the yield strength.

$$\delta_Y = (A + B\bar{\varepsilon}_p^n)(1 + Cln\dot{\bar{\varepsilon}}_p^*)(1 - T^{*m}) \qquad Eq.7$$

$$\dot{\bar{\varepsilon}}_p^* = \frac{\dot{\bar{\varepsilon}}_p}{\dot{\bar{\varepsilon}}_0} \qquad T^* = \frac{T - T_A}{T_M - T_A}$$

While $\bar{\varepsilon}_p$ gives the equivalent plastic strain, $\dot{\bar{\varepsilon}}_p^* = \dot{\bar{\varepsilon}}_p / \dot{\bar{\varepsilon}}_0$ is the dimensionless plastic strain rate for $\dot{\bar{\varepsilon}}_0 = 1.0 \ s^{-1}$. T^* gives homologous temperature while T_M is melting temperature and T_A is the ambient temperature. A, B, C, n and m are constant parameters specific for materials; where A is the room temperature yield strength, B is the strain hardening constant, n is the strain hardening exponent, C is the strain rate constant and m is the thermal softening exponent. Constant were taken from standards [52] and given in Table 11.

Table 11: Johnson – Cook constitutive law coefficients of 6063 – T6 aluminum alloy [52]

	A (MPa)	B (MPa)	n	C	m	$T_M(^oC)$
6063 – T5	324	114	0,42	0,002	1,34	651,85

Failure criteria of Johnson – Cook Model is based on a plastic fracture strain and defined in the equation 8. [51]

$$\bar{\varepsilon}^f = [D_1 + D_2 \exp(D_3\tilde{\sigma})][1 + D_4 ln|\varepsilon^*|][1 + D_5 T^*] \qquad Eq.8$$

where $\bar{\varepsilon}^f$ is plastic fracture strain and $\tilde{\sigma}$ is the triaxiality strain rate. The specific material parameters D_1, D_2, D_3, D_4 and D_5 are determined from tests under different triaxiality. The constants specific for material $6063 - T6$ is shown in Table 12.

Table 12: Johnson – Cook Failure model material constants of 6063 – T6 aluminum alloy [52]

	D_1	D_2	D_3	D_4	D_5	$T_M(^oC)$
6063 – T5	-0.77	1.45	-0.47	0	1.6	651,85

Failure occurs when the damage variable D reaches the value 1. $\Delta\varepsilon_p$ is increment of the von Mises equivalent plastic strain and is found by the integration in equation 9.

$$D = \sum \frac{\Delta\varepsilon_p}{\bar{\varepsilon}^f} \geq 1 \qquad \bar{\varepsilon}_p = \int \dot{\bar{\varepsilon}}_p dt = \int \sqrt{\frac{2}{3}\dot{\varepsilon}_{ij}^{dev}\dot{\varepsilon}_{ij}^{dev}}\,dt \qquad Eq.9$$
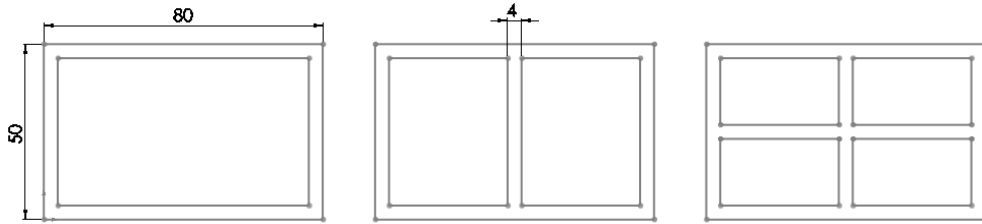
Figure 25: Different cross – sections of S – shaped aluminum profiles that were subjected to the dynamic impact analysis

For impact test simulation of aluminum extrusion profiles three cross-sections were selected which are shown in Figure 25. All cross – sections had the same outside dimensions as 80 x 50 mm with a thickness of 4 mm. The analyses were carried out via using ANSYS 13 – Workbench Explicit Module. Engineering data and Johnson – Cook Model parameters were applied to the models. Profiles with a different cross – sections were designed as S – shaped to simulate the frontal impact members as close to reality. The dimensions of the S – shaped profile is shown in Figure 26. The total length of the profile was 780 mm with curvature angles of 45º. Mass was attached to the rare part of the profile as a rigid body with a density of $7x10^7$ which gave 500 kg

load which is the possible weight distribution during crash for each frame. Meshing was done with maximum mesh size to investigate stress and deformation regions clearly. Hexahedral and quadrilateral element types were chosen which are more suitable for non-linear analysis. The front part of the profile with an initial velocity hits a rigid wall in order to simulate the dynamic crash conditions. The initial velocity was applied to the rigid body which was bonded to the frame as 11.11 m/s (40 km / hour) in the x - direction. The total analysis was carried out for 0.05 seconds. The aim on this simulation was to analyze the impact reaction of the S – shaped profiles associated with real crash dynamics.
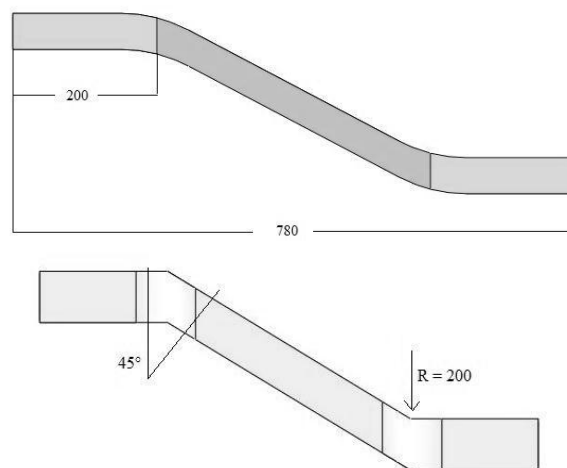
Figure 26: Dimensions of S – shaped aluminum profiles (up) right – view, (down) top - view

Time was selected according to collision calculations. If the car hitting the wall with a speed of 120 km/h (33,528 m/s), it stops until the velocity become zero while the deformation is occurred in crumple zones. Deceleration was assumed as 60 g (588 m/s^2) which is maximum average long duration acceleration limit that is specified by NHTSA (National Highway Traffic Safety Administration). From the basic physic formula, Velocity = Time x Acceleration, time can be calculated as 0,057 seconds for an accident at 120 km/h. [53]

Energy absorption of profiles during crash was obtained from the loss in kinetic energy. Specific energy absorption which is a measure of absorbed energy per mass

47

was calculated and results were compared between three cross – sections. On the other hand, peak forces of each cross – section were also determined which is expected as small as possible. Because when the peak force is high, force is transmitted to the passenger during the collision which may be hurtful. Peak force of each profile was calculated by the contact force during collusion. The suitable cross-section of aluminum extrusion profile were determined from analyses and produced according to the results of specific energy absorption and peak forces.

CHAPTER 4

RESULTS AND DISCUSSION

4.1 Sand Casting Results

4.1.1 Alloy Selection

Spiral fluidity test results are shown in Table 13. As it is known, fluidity is increasing with increased silicon content in aluminum alloys. So experiment results were observed as it was expected from literature. (Figure 27) B390.0, according to the highest Si content, showed the maximum fluidity compared to the other alloys. Despite A413.2 is the second alloy with high Si content through containing 12% Si, flow length was not long enough as it is expected. Also A413.2 is a die cast alloy and it may show different behavior in sand casting.

Table 13: Flow lengths of candidate aluminum alloys in sand casting

Alloy	Flow Length (cm)
A356.0	82
A357.0	81
B390.0	86
A413.2	80
Silafont - 36	84

Figure 27: (left) The model of spiral fluidity that was used in sand molding, (right) spiral cast of A390.0 alloy after pouring

Besides the fluidity, mechanical properties of aluminum alloys are also important. For this reason B390.0 alloy was eliminated according to its low ductility because the selected alloy will be in use for parts that are exposed to impact loads. When compared flow lengths and mechanical properties between candidate aluminum alloys, A.356.0 and Silafont – 36 were given the best combined results.

In order to compare the mechanical properties of A356.0 and Silafont – 36 to select the most proper alloy for our experiments, tensile tests were done and results are shown in Table 14 and Figure 28. All results were obtained lower than literature because of some problems during molding and casting process as surface defects and porosity. Especially a big reduction in mechanical results at Silafont – 36 compared to literature was observed because of sand mold casting was done despite it is a die cast alloy.

Table 14: Tensile test results of A356.0 and Silafont – 36 aluminum alloys

	A356.0		Silafont - 36	
	UTS (MPa)	Elongation (%)	UTS (MPa)	Elongation (%)
Test 1	137	3	207	4.1
Test 2	150	1.8	223	4.2
Test 3	146	2,5	211	2.9
Mean	144.3 ± 6.65	2.43 ± 0.6	213 ± 8.32	3.73 ± 0.72

50

Higher ultimate tensile strength was determined in Silafont − 36 with its higher silicon content when compared with A356.0. On the other hand, higher elongation results were also obtained in Silafont − 36 because of its low iron content so the brittle intermetallic $FeAl_3$ phase was hindered. When all results were taking into account, Silafont − 36 was given higher mechanical properties than A356.0 in addition to its higher fluidity.
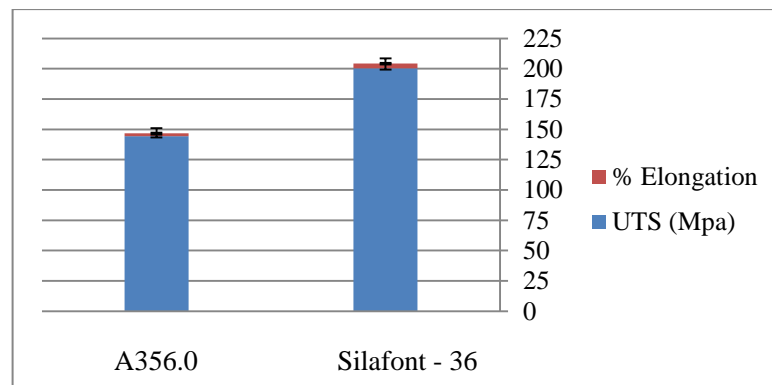
Figure 28: Comparison chart of mechanical properties of A356.0 and Silafont − 36 after tensile test

4.1.2 As Cast Parts

An aluminum silicon alloy having low iron content was prepared for chassis parts. Spectrometer result of aluminum alloy composition that was used in our study is shown in Table 15. As it is seen from table, composition was observed similar to the trademark aluminum alloy Silafont - 36. 16 parts which are shown in Figure 29 were produced with using this alloy by sand casting process. Standard deviation was calculated and each element percentage was found between the appropriate values.

Table 15: Chemical composition of Silafont − 36 aluminum alloy that were used in production taken from spectrometer

	Si	Fe	Cu	Mg	Ti	Sr
% Alloy	10.3	0.12	0.04	0.29	0.14	0.018
Deviation	± 0.46	± 0.008	± 0.005	± 0.03	± 0.01	± 0.002

Figure 29: As cast parts of space frame with Silafont – 36 aluminum alloy and their patterns; a) A-pillar, b) B-pillar, c) C-pillar, d) front frame support, e) rare frame support (continued)

Figure 29: As cast parts of space frame with Silafont – 36 aluminum alloy and their patterns f) fender support, g-h) shock absorber tower, i) parts in assembly at space frame

Cooling curves after thermal analysis are shown in Figure 30. The eutectic solidification time and growth temperature are shown in Table 16 where Te is the eutectic temperature, ΔTe is the eutectic undercooling and ΔTn is the liquidus undercooling. Also dT/dt curves which were calculated from the first derivative of thermal analysis results are shown in Figure 31. As seen from the graph, undercooling of nucleation of primary α phase is getting smaller as the grain refiner added. Without refinement, the growth temperature of liquidus must be below the nucleation temperature for the spontaneous formation of nucleation. Due to this reason while the undercooling was 1.8ºC in untreated Silafont-36 alloy, it was lowered to 1.2ºC after AlTi5B1 addition. This value was reached to zero after modification. The eutectic temperature was 573.8ºC which lasts 57 seconds and also the eutectic undercooling temperature was 0.1 ºC. After modification with AlSr10, eutectic temperature was suppressed by 2.9ºC (571ºC). On the other hand the eutectic solidification time was significantly extended and took place in 160 seconds. These results were indicated that grain refinement and modification was done succesfully.
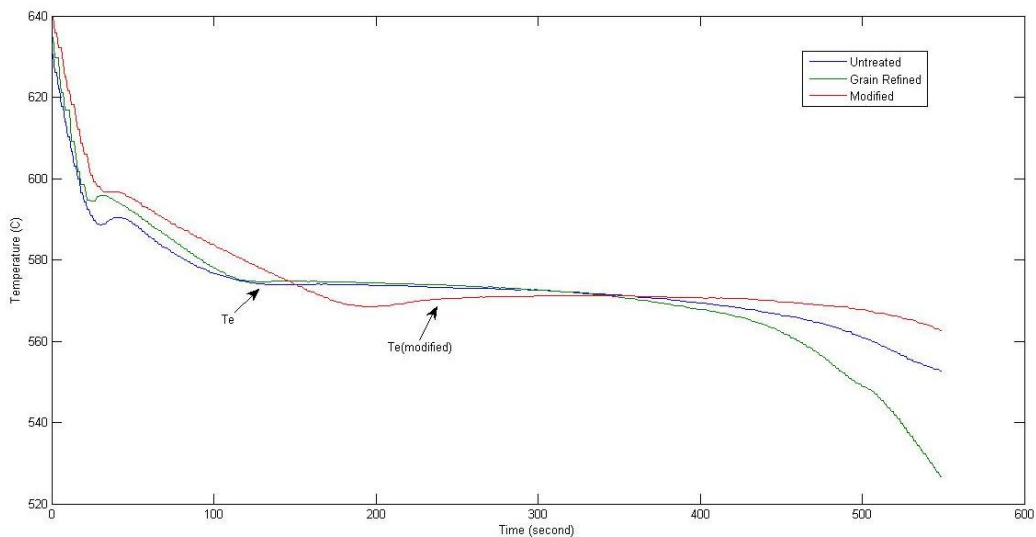
Figure 30: Cooling curves of Silafont – 36 untreated, after grain refinement and eutectic modification

Table 16: Solidification time and temperatures for each treatment

	Te (°C)	Time (s)	ΔTe (°C)	ΔTn (°C)
Untreated	573.9	57	0.1	1.8
Grain Refined	574.7	29	0.2	1.2
Modified	571	160	2.6	0
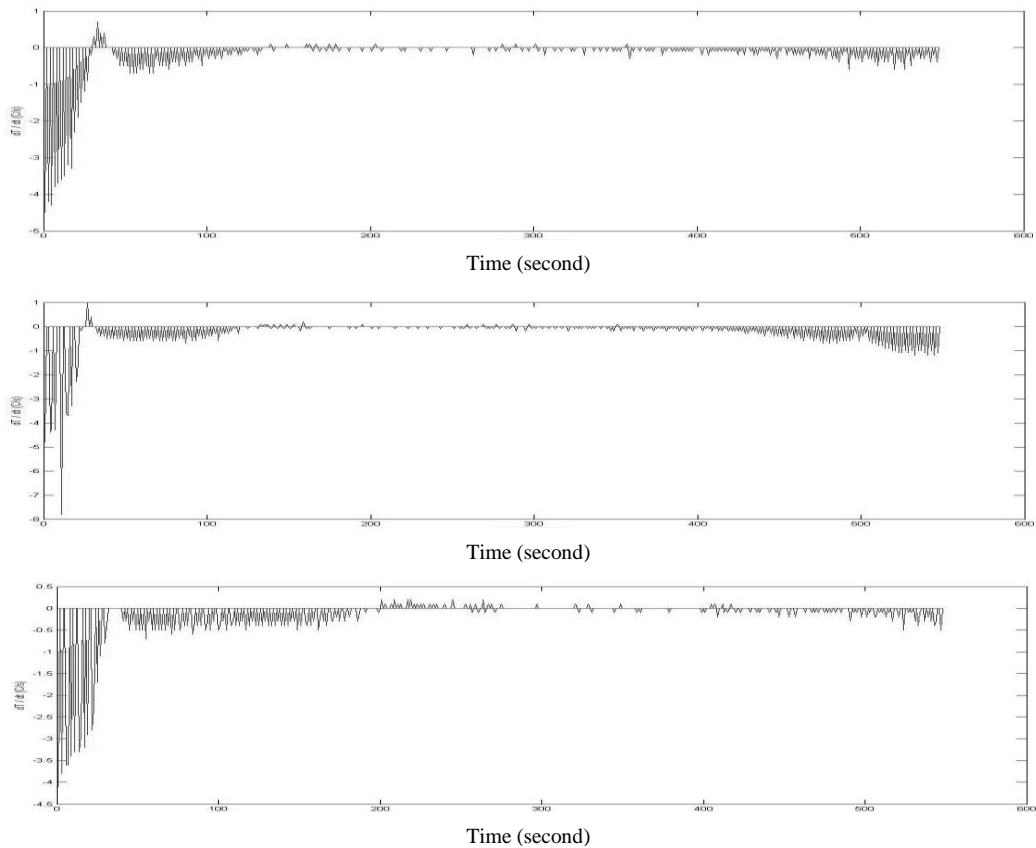
Figure 31: First derivative of cooling curves a) untreated, b) after grain refinement, c) after modification

Microstructures of unmodified and modified sand cast Silafont – 36 are shown in Figure 32. Micro analysis was carried out to determine modification effect on eutectic Al – Si aluminum alloy. While in unmodified casting the majority of microstructure contains coarse silicon plates as seen from the Figure 32 (left), with Sr addition particles were formed into finer and spherical (right). The fibrous silicon particles in the microstructure demonstrated the modification was sufficient in Al – Si alloy.
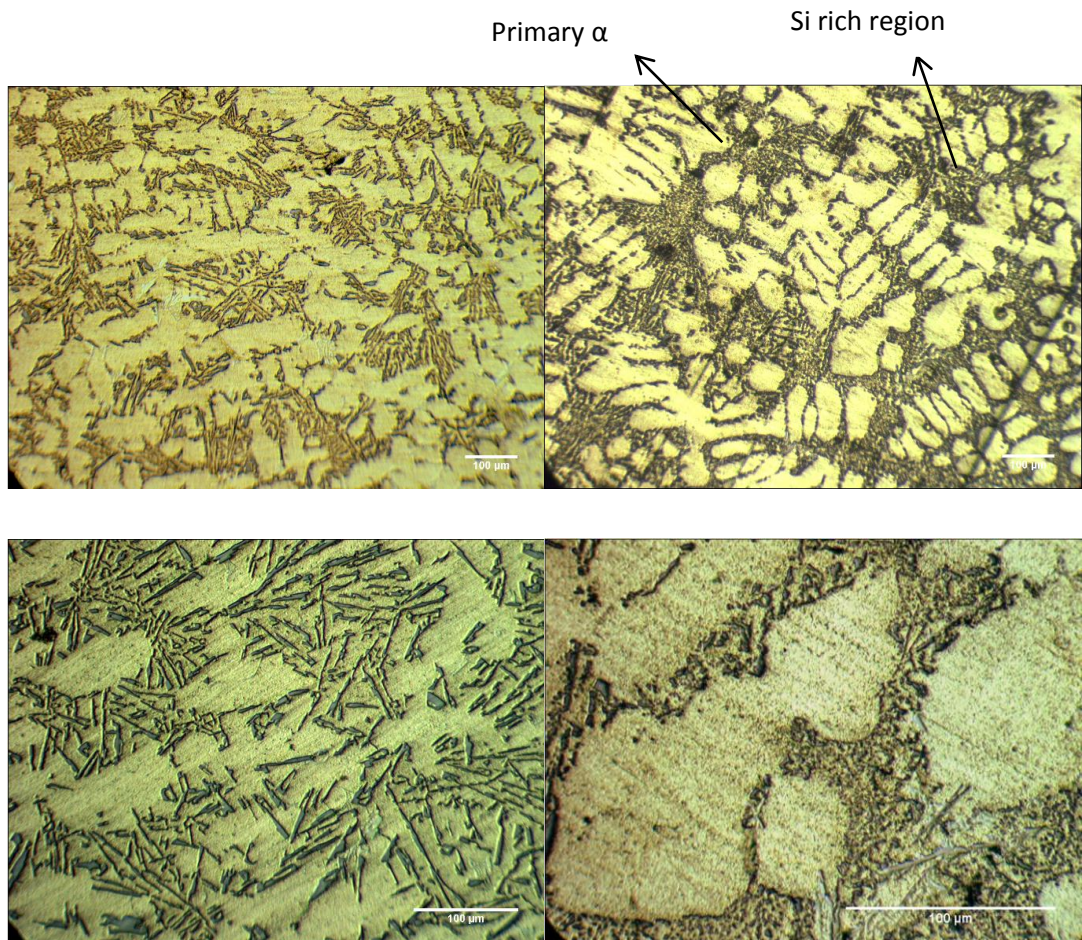
Figure 32: Light microscopy images of the sand cast Silafont – 36 aluminum alloy samples (etched with Keller); top) 100x magnification, bottom) 200x magnification

4.1.3 Mechanical Properties Evaluation with Heat Treatment

Hardness curve with changing heat treatment time is shown in Figure 33. As it is seen from the graph, 3 hours solutinizing time and 6 hours aging time was the best combination and gave the maximum Brinell hardness results which are shown in Table 17. Below the 3 hours of solutinizing, there was not enough time for all Mg_2Si precipitates to dissolve in solution and homogenous phase cannot be obtained. Above 3 hours, grains became longer and reduction in mechanical properties was observed. Even different solutionizing times were occurred, all three curves has shown the peak positions after aging for 6 hours. Then hardness was decreased with the over aging because Mg_2Si precipitates were became coarser and agglomerated in grain

boundaries. The maximum Brinell hardness results were still lower than the theoretical when compared with the Silafont – 36 since the production process was different according to use of sand casting. Nevertheless, all results were sufficient to use in chassis parts.

Table 17: Brinell hardness results at each solutinizing and aging treatment of sand cast Silafont-36

T4	2 Hours				3 Hours				4 Hours			
T6	Specimens (HB)			Err	Specimens (HB)			Err	Specimens (HB)			Err
4hr	54.4	59.6	56.8	2.12	62.7	63.3	61.1	0.92	60.2	58.6	62.8	1.73
5hr	57.3	58	57.8	0.29	71.7	68.1	70.7	1.51	63.1	58.8	64.4	2.39
6hr	63.1	62.1	62.4	0.41	69.3	72.2	70.1	1.22	66	62	61.4	2.04
7hr	60.5	56.4	57.9	1.69	65.5	65.3	64.9	0.24	60	58.4	58.7	0.69
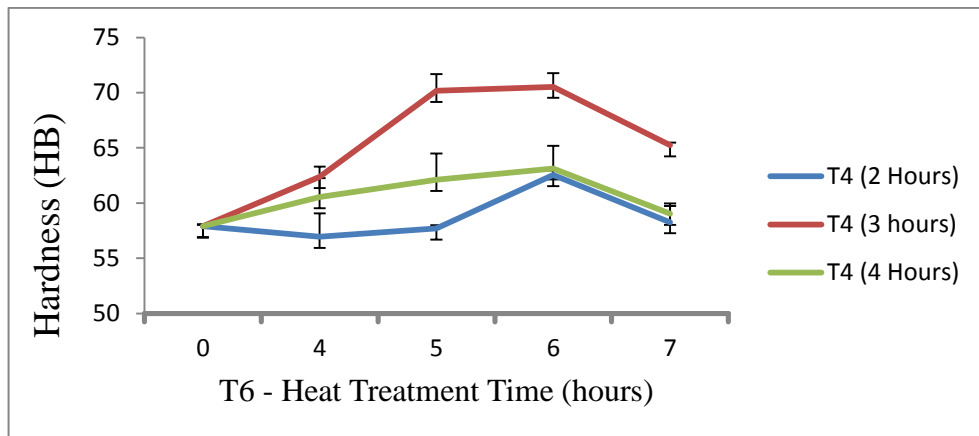
Figure 33: Hardness curve with changing artificial aging heat treatment time of sand cast Silafont - 36

Tensile test results are shown in Table 18. It is clear that the lowest elongation was found in fabricated samples because of improper precipitate dispersion and stress formation in structure during casting. Due to this reason, parts must be subjected to any heat treatment after casting to obtain sufficient ductility. After the solutionizing and annealing treatments while the ultimate tensile strength kept the same values, elongation was increased in higher ratios. The best improvement in ultimate tensile

strength with a sufficient elongation was observed with artificial aging heat treatment. Compare to the samples which were not subjected to heat treatment, the samples subjected to T6 heat treatment the ultimate tensile strength was increased 21%, elongation was increased twice of the samples. The reason of the improvement of mechanical properties with T6 heat treatment was the proper dispersion of fine Mg_2Si precipitates in α phase. Standard deviation of each experimental result was obtained low enough to make accurate measurements and comparison.

Table 18: Tensile test results of different heat treated sand cast Silafont - 36

	UTS (MPa)			Elongation (%)			
Treatment	Test Results		Mean	Test Results			Mean
F	178 174 177		176±2.08	1.36	1.37	1.36	1.36±0.005
O	160 154 162		158±4.16	5.31	5.26	5.3	5.29±0.02
T4	171 165 152		162±9.71	4.8	4.6	4.08	4.49±0.37
T6	223 207 211		213±8.32	4.2	4.1	2.9	3.73±0.72

Charpy impact test results are shown in Table 19. Due to the sand casting, low absorbed energy values were obtained for all samples because of very low cooling rate. Despite the annealed samples had the highest elongation, they did not give the maximum energy absorption. Samples which were subjected to T4 heat treatment absorbed the maximum energy. The elongation and energy absorbance difference for same heat treatments can be occurred because of surface defects and porosity. Due to brittle behavior of fabricated samples, they absorbed less energy. Besides the sufficient tensile test results was obtained by T6 heat treatment, impact energy absorbance was also increased 60% (3.62j) compared to the untreated samples. Samples failed in impact test are shown in Appendix A. Also the relationships between impact test results and tensile test results are shown in Figure 34.

Table 19: Charpy impact test results of different heat treated sand cast Silafont - 36

Treatment	Impact Energy Absorbance (J)				Mean
F	5	7	6.5	5.5	6 ± 0.79
O	12.5	10.5	11	12	11.5 ± 0.79
T4	15	13.5	14	14.5	14.25 ± 0.55
T6	9	8.5	11	10	9.62 ± 0.96
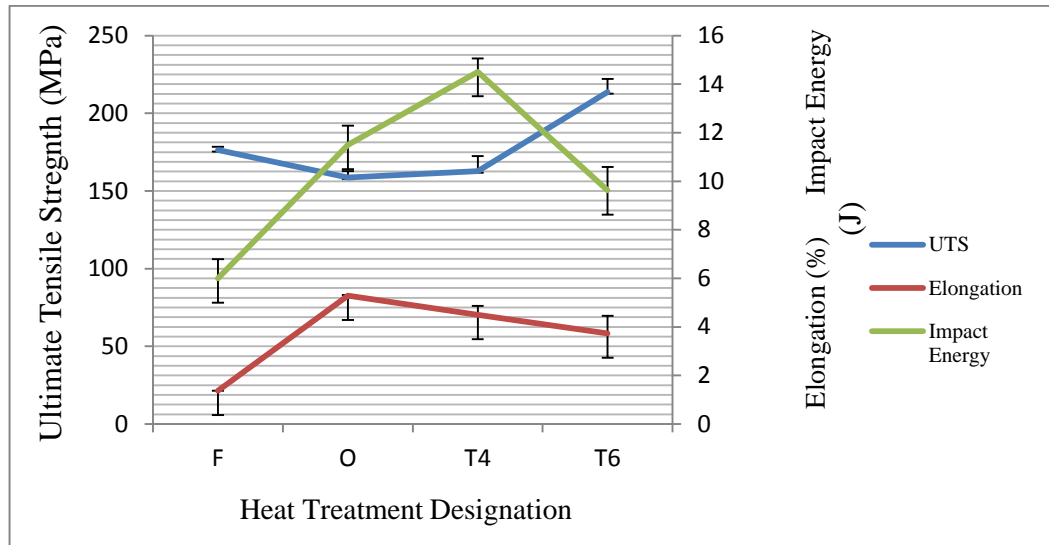
Figure 34: Ultimate tensile strength, elongation and charpy impact energy change with different heat treatments

4.2 Extruded Profiles

4.2.1 Hardness – Heat Treatment Curve Results

Extruded profiles that were directly subjected to the aging process at 185ºC with different times are shown in Table 20 and the curve of hardness change against heat treatment time is shown in Figure 35. While hardness of profile without any heat treatment had an approximately 47 HB, the curve has reached to top value at 73.1 HB which was so close to the theoretical value as 74 HB. The maximum hardness was achieved when aging was applied between 5 - 7 hours. When the sufficient time was allowed, hardness was not changed significantly and over aging was not observed until 20 hours.

Table 20: Brinell hardness test results at different T6 heat treatment times

Heat Treatment (T6) Time (hours)	Test 1 (HB)	Test 2 (HB)	Test 3 (HB)	Mean (HB)
0	48.9	46.4	47.9	47.7 ± 1.02
2	58.3	58.3	57.9	58.1 ± 0.18
4	70	67.4	68	68.4 ± 1.11
6	74.1	72.8	72.4	73.1 ± 0.72
8	69.4	70	67.8	68.4 ± 1.14
10	68.1	68.8	69.4	68.7 ± 0.53
12	66.9	68	68	67.6 ± 0.51
14	67	67.6	66.1	66.9 ± 0.61
16	67.4	67.4	67.8	67.5 ± 0.18
18	70	71	66.3	69.1 ± 2.02
20	69.1	71	68.6	69.5 ± 1.03
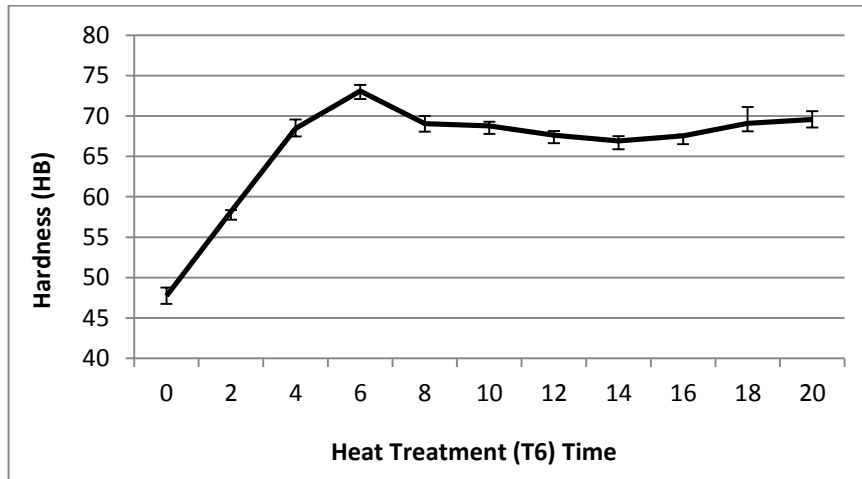
Figure 35: Curve of hardness change with T6 heat treatment of 6063aluminum alloy

Extrusion samples which were solutionized at 520ºC for 8 hours and quenched at room temperature were shown in Table 21 and Figure 36. Even the fabricated sample and theoretical hardness of untreated profile was 47 HB and 46 HB respectively, after solutionizing the value was increased above 50 HB. But aging at 205ºC for several hours hardness was not high and values were lower compared to the samples subjected to T6 heat treatment. The maximum hardness level was reached to 57.4 HB

when aging was done for 2 hours. Comparing the results of the samples subjected to T5 and T6 heat treatments, higher hardness was obtained by aging process carried out as T6 condition at lower temperature as 185ºC.

Table 21: Brinell hardness test results at different T5 heat treatment times

Heat Treatment (T5) Time (hours)	Test 1 (HB)	Test 2 (HB)	Test 3 (HB)	Mean (HB)
0	48.9	46.4	47.9	47.7 ± 1.02
1	52.1	50.5	51.3	51.3 ± 0.37
2	54.3	56.9	58.6	56.6 ± 0.88
3	53.1	57	54.1	54.7 ± 1.24
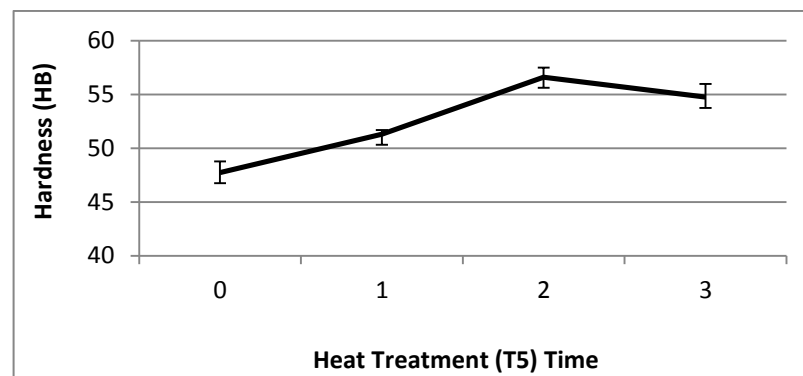
Figure 36: Hardness change curve with T5 heat treatment of 6063aluminum alloy

4.2.3 Three Point Bending Test Results

Three point bending test results of extruded profiles were obtained from tensile testing unit load − displacement curve is shown in Figure 37. As seen from the curve, aluminum profiles can be replaced with steel profiles in chassis under the condition of maximum load. Heat treated aluminum profiles were started to deformation under higher loads approximately at 5000 kg. Also it is not surprising that displacement value is highest at T4 heat − treated aluminum profiles. Strain was determined 20%

in T4 heat-treated and 18% in T6 heat-treated aluminum profile which was close to the theoretical values. While the highest peak load was obtained as 85kN at 6063 – T6 profile, low carbon steel profile had the lowest peak load with 46kN.

Energy absorption was calculated from the area under the curves. Besides absorbed bending energy of carbon steel profiles was 2161 joule, untreated and heat-treated aluminum profiles were showed energy absorbance twice as much steel, 4182 and 4927 joule respectively.
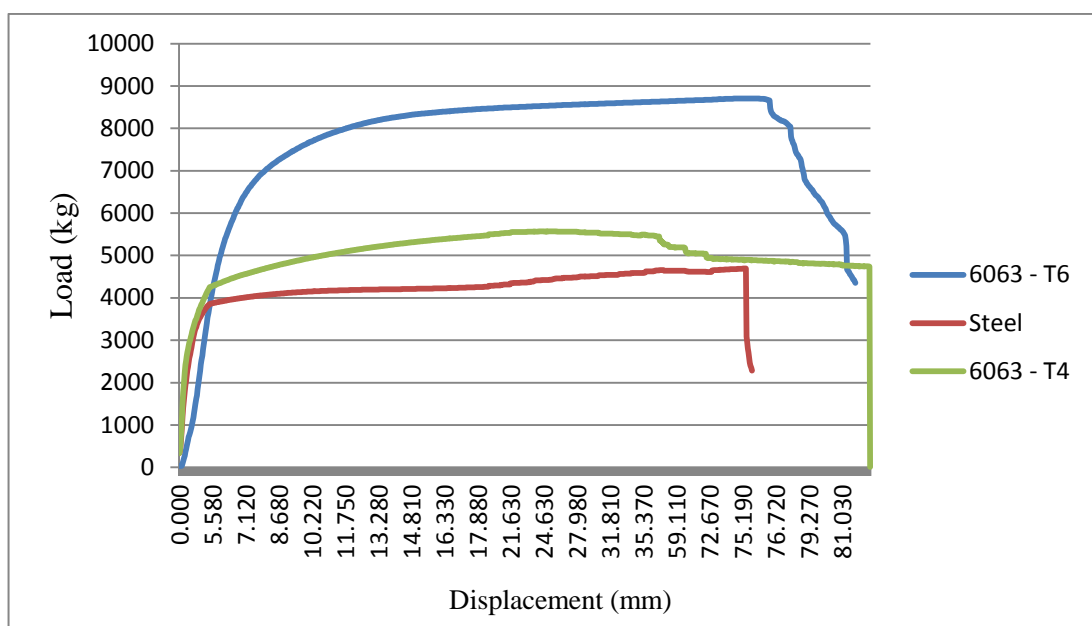
Figure 37: Load – displacement curve of aluminum and steel profiles that were subjected to 3 – point bending test

There was a visible fracture at bottom part of the 6063 – T6 profile in a direction perpendicular to the extrusion direction during three-point bending until the intender had almost reached its complete displacement. (Figure 38) The fracture was occurred because of the high stress intensity and it was consisted from the support part of profile which makes a shear stress during bending load. In addition to the fracture of 6063- T6, 6063 – T4 profile showed a surface cracks and fracture underneath the upper intender in a parallel direction. Cracks in 6063 – T4 did not occur until after the peak load had been attained. In low carbon steel profile, no visible fracture was

observed and cracks were occurred similar to the 6063 − T4 profile underneath the upper intender in a parallel direction. Deformed aluminum and steel profiles are shown in Appendix B.

Figure 38: Deformed T6 heat treated profile view after 3-point bending test

4.2.4 Moment of Inertia Results

The equation 12 was used to determine the bending moment (M);

$$M = \frac{P.L}{4} \qquad \text{Eq.12}$$

where P is the bending force and L is the length of the profile. L becomes L/4 when the force was applied from the center point of profile in three point bending test. P was assumed as the load that plastic deformation started to provide maximum load durability of materials and work in safety region.

Yield strength and ultimate tensile strength of materials according to the different cross − sections were obtained and results are shown in Table 22. When the shear stress was considered because of support part of the aluminum profile during bending, yield strength value was decreased and became closer to the theoretical. It is not surprising that steel shows higher yield strength in comparison with aluminum. But with changing cross − sections, higher moment of inertia was obtained with

aluminum profiles and in this way higher resistance to plastic deformation was provided despite lower yield tensile strength of aluminum. Ultimate tensile strength of aluminum was obtained similar to the steel. Despite low carbon steel has higher modulus of elasticity (205 GPa) than aluminum alloy (69 GPa), the moment of inertia results with changing cross-section and thickness of aluminum which was twice as steel, so 6063 aluminum alloy can be replaced with low carbon steel under safety region.

Table 22: Calculated mechanical properties of aluminum and steel profiles with different cross - sections

	Moment of Inertia (mm^4)	Yield Strength (MPa)	Ultimate Tensile Strength (MPa)
Low Carbon Steel (Square)	147713	304	318
Aluminum (6063 – T6) (Supported)	413501	222	330
*With Shear Stress	413501	197	206
Aluminum (6063-T6)(Vertical)	1858205	250	340

4.3 Mechanical Properties Results of Welded Samples

Fabricated and heat treated sample results after welding are shown in Figure 39. Samples which were directly used after extrusion showed the lowest hardness at heat affected zone (HAZ) and parent metal. But hardness change was not in wide range; only a small decreasing at HAZ as 46 HB and the parent metal was approximately 50 HB. In the artificial aged samples, hardness was decreased significantly at HAZ as we mentioned before in literature. It is a typical 6xxx series hardness graph after welding and this hardness was observed because of precipitation dissolution. Hardness reduction was continued approximately 20 mm away from welding pool which is the HAZ region of this sample. On the other hand, samples which were heat treated after welding did not show any significant change in hardness. After parent metal was heated up to the elevated temperature with welding and precipitates were dissolved, aging was assisted to re-disperse precipitates as a fine distribution.

HAZ region became shorter than heat-treated samples with a 15 mm away from welding pool. But aging process was not suitable after welding because of complex and large assemblies and furnace capacity, in this reason heat treatment was done before welding for each part in our experiments. Sand cast samples were given the similar curve as extruded samples and decrease in hardness was taken place 18 mm away from weld seam. But hardness of weld seam and parent metal was higher than the other ones. While the weld seam was 55 HB in extruded samples, it was 62 HB in sand cast samples.
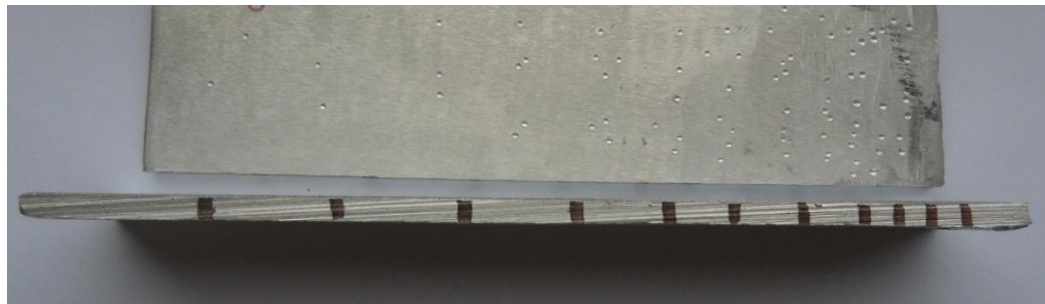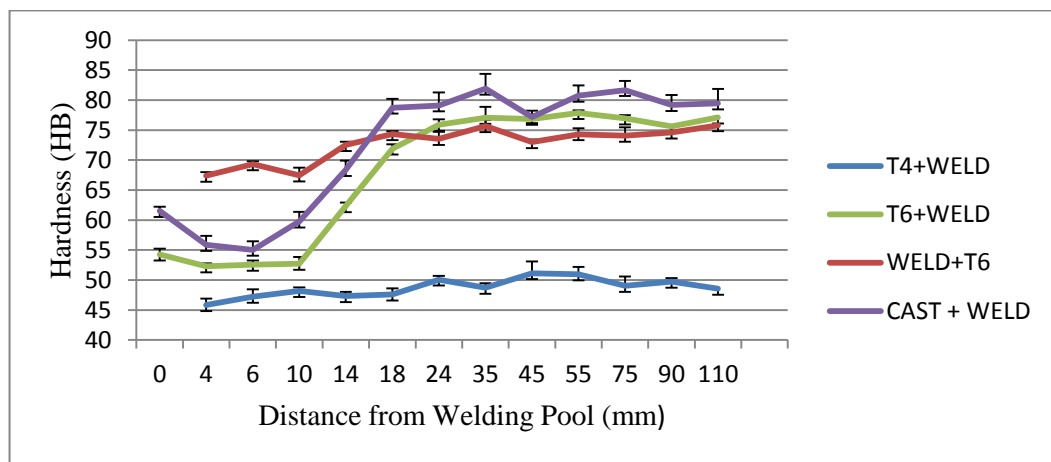
Figure 39: (top) Hardness curves of heat affected zones at different heat treatment processes, (bottom) Samples that were used for hardness test

The hardness was taken after 1 month and 3 months from the welded sample following the T6 heat treatment is shown in Figure 40. As seen from the chart, curves were begun to rise earlier with time passing. When a period of time was passed, an increase in hardness was seen with the start of the natural aging process. There was

not significant increase close to the weld seam after 3 months. But hardness was started to increase in short distances as 17 mm and 13 mm after 1 month and 3 months was passed respectively. Also, specimen was held in furnace at 50ºC for 3 days to determine the changing on hardness curve and as a result increment took place in a shorter time. So when the chassis frames are exposed to the higher temperatures than the room temperature under the sunlight, hardness is increased faster at heat affected zone with the increasing rate of natural aging. As it is seen from the graph, hardness was increased in heat affected zone, over aging was not still observed at the parent metal. (Figure 41)

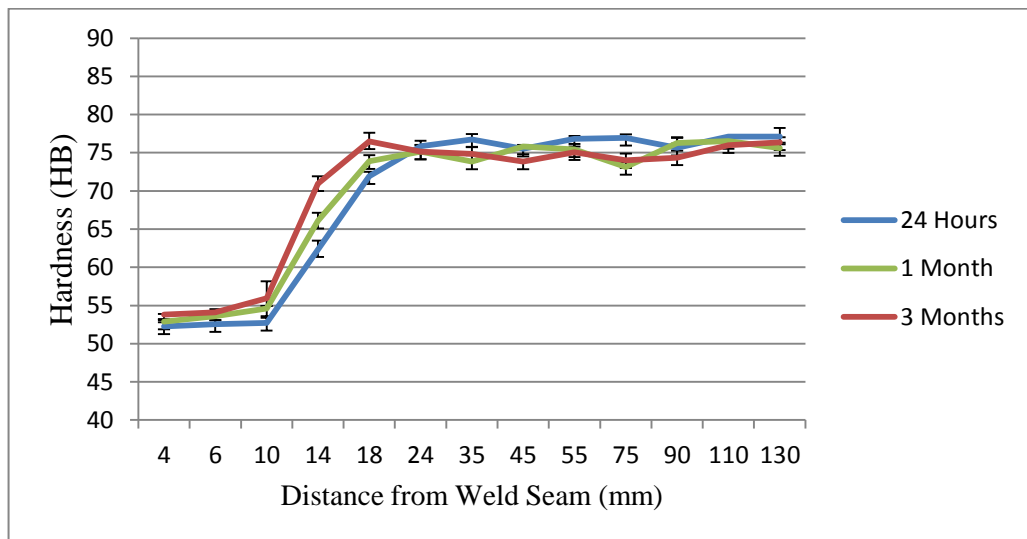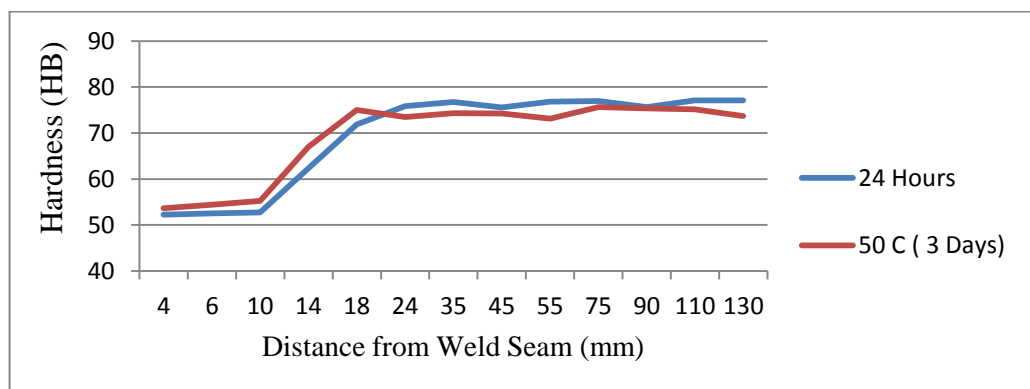Figure 40: Hardness curves of heat affected zones after welding at various times

Figure 41: Hardness curve change of heat affected zone at 50ºC for 3 days

Tensile test results of welded specimens are shown in Table 23. As it was expected, the ultimate strength and elongation values were decreased with low ductility because samples were exposed to heat during welding. When two extruded plates were welded together, failure occured from the weld seam which means it was the weakest region of welded parts. The deviation of elongation was found high because of the possibility of hot cracking which is a typical problem in 6xxx series of aluminum alloys. Plastic deformation was also started above 800 kgf and when the welding of assembly is considered to be sufficient but still low. On the other hand, results of welding between extruded and sand cast plates were higher than the extruded samples. Elongation was also observed more uniform. Some samples were failed during the test because of sand defects inside of the cast parts. Fracture was occurred at the parent metal from the extruded side. Also this situation was proved with the hardness difference between weld seams in extruded and sand cast samples. Consequently, the weakest region was became the extruded plates with their lower silicon content and plastic deformation was started above 1000 kgf. The fracture view of tensile test samples is shown in Figure 42.

Figure 42: Welded samples after failed in tensile test, (top) extruded – extruded sample, (bottom) extruded – sand cast sample

Table 23: Tensile test results of welded samples

	Extrusion – Extrusion		Extrusion – Sand Cast	
	UTS (MPa)	Elongation (%)	UTS (MPa)	Elongation (%)
Test 1	111	4	126	5.4
Test 2	93	4.3	117	5.7
Test 3	113	3.4	122	6.37
Test 4	76	5	100	5.21
Test 5	95	1.88	118	5.17
Mean	97.6 $\pm$ 15.09	3.71 $\pm$ 1.17	116.6 $\pm$ 9.93	5.57 $\pm$ 0.49

In Figure 44, images of welded samples were taken by light microscope at 100x and 200x. 4043 aluminum alloy was used as a filler metal which contains 5.2% silicon. Silicon particles were diffused to the weld pool during welding and as it is seen from the microstructures, the silicon content of weld seam was increased and semi-eutectic microstructure was achieved at the sand cast side. EDX analysis was done at weld seam to figure out the changing in silicon content after welding. Line scans were held with several points at weld seam. As shown in Figure 43, silicon content was higher in the filler metal at weld seam when sand cast and extrusion samples were welded together. During the welding, the high silicon content (9-11%) of sand cast part was mixed with the filler alloy (5.2%) and increased the percentage of silicon in welding pool. In the same way, when extruded samples were welded together, silicon particles were diffused to the lower silicon content which was the parent metal and the silicon content of weld seam was decreased.
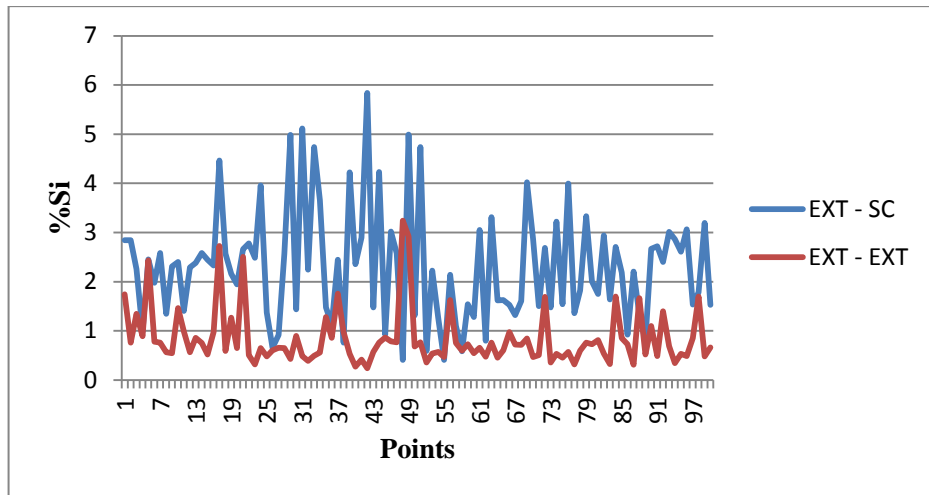
Figure 43: EDX line scan analysis of welded parts from weld seam section
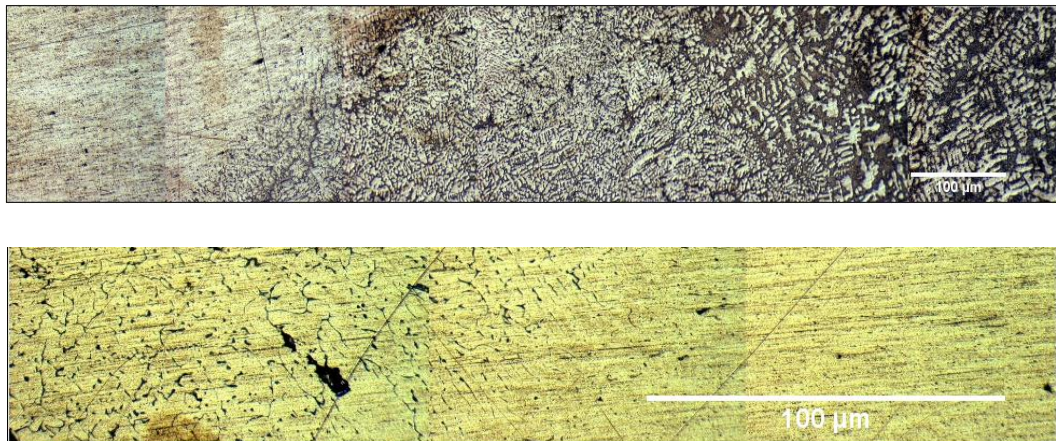
Figure 44: Light microscopy images of the weld seam and parent metals. (top) Microstructures of extruded, weld seam and sand cast sections respectively (100x, no etching), (bottom) weld seam and extruded section (200x, etched with Keller)

4.4 Finite Element Analyses Results

4.4.1 Static Analyses

Bending analysis results of aluminum space frame were evaluated with using finite element method. In analyses, sheets and other parts to be added were ignored and zero stiffness addition was assumed. Stress distribution was investigated and frontal

S-shaped profiles were became most exposed parts for bending moments. Although stress was mostly seen in these frontal parts, they were still below the critical stress limit with approximately 100 MPa against 2000 kg load. After fatigue analysis was done, frontal s-shaped profiles, midpoint and rear point of sill became in safety region which is shown in Figure 45. Furthermore when sheet parts addition is considered, the safety factor of these regions will be also increased.
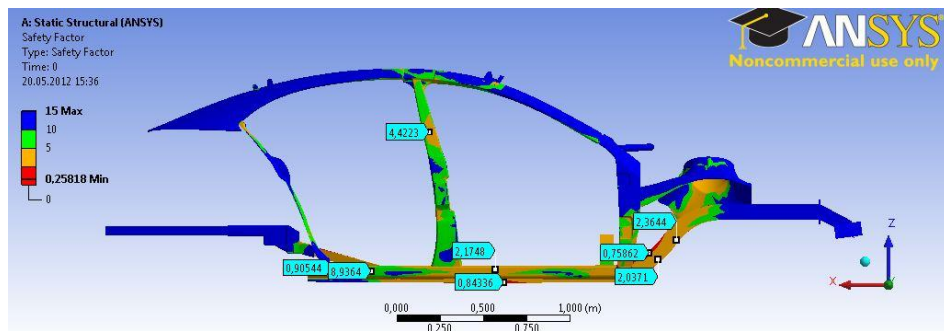
Figure 45: Safety factor results of bending stiffness analysis against 2000 kg

First torsional analysis method was done to determine torsional stiffness of space frame chassis. Body was fixed from rare part and equal loads were applied in opposite direction to the shock absorbers as it is seen in Figure 46. Analysis was carried out 1 second and several loads were applied from 1000 N.m to 5000 N.m (with increments of 500 N.m). Safety factor, for 10^9 cycles of design life, was not so critical under 4000 N.m torque for each point and damage was started from mounting locations with increasing torque above 4000 N.m.
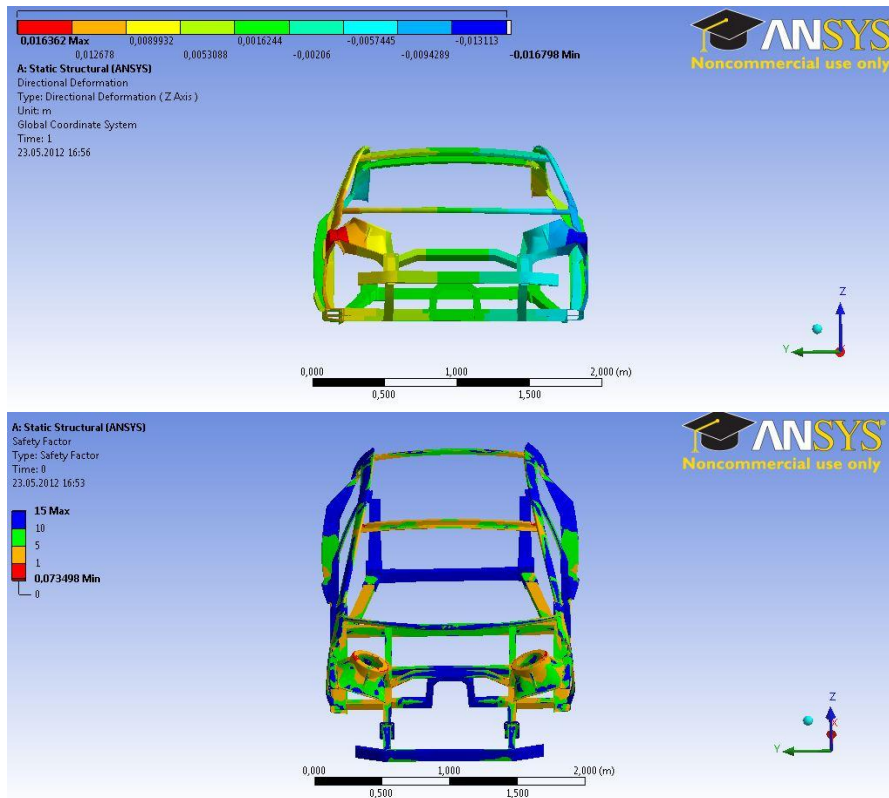
Figure 46: Deformation at Z – axis (a) and safety factor results (b) after torsional stiffness analysis against two moments at the mounting locations of shock absorber

After simulating all analyses, the overall torsional stiffness was calculated with using equation 5 and found approximately 5153.782 N.m/deg. Distance between two mounting locations and stiffness energy for each torque is given at Table 24. Because of many structural members were missing, torsional stiffness was found under typical vehicles which is between 7 – 20 kN.m/deg. Applied torque versus deflection were taken into chart which can be seen in Figure 47 and torsional stiffness was found linear as it is expected.

71

Table 24: Deformation and stiffness results of torsional stiffness analysis

Torque (N.m)	Deflection (m)	Distance (L) (m)	θ (degree)	Stiffness Energy (joule)	Torsional Stiffness (N.m / deg)
1000	0,001946	1,15	0,194036	17,82	5153,673
1500	0,002920	1,15	0,291058	40,042	5153,609
2000	0,003893	1,15	0,388078	71,243	5153,6
2500	0,004866	1,15	0,485086	111,73	5153,723
3000	0,005839	1,15	0,582101	163,38	5153,742
3500	0,006812	1,15	0,679113	220,86	5153,781
4000	0,007785	1,15	0,776111	297,06	5153,902
4500	0,008759	1,15	0,873114	377,99	5153,964
5000	0,009732	1,15	0,970113	469,44	5154,039
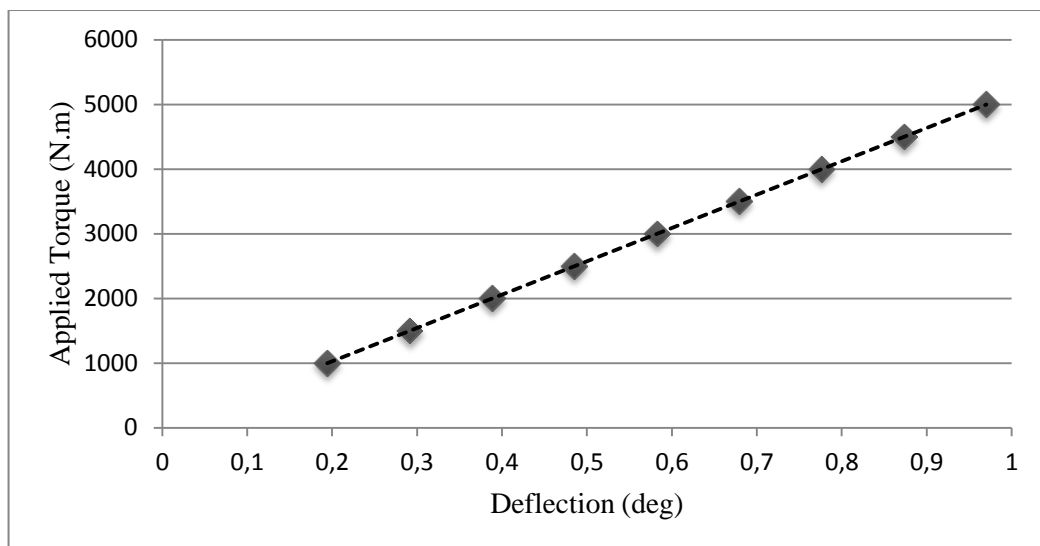
Figure 47: Deflection degrees against applied torque

In second torsional analysis method that the chassis was fixed from its three points and load was applied to the shock absorber tower was done to simulate when the single wheel fall into the pit and load is transmitted to the chassis from shock absorber. There is no critical stress distribution was shown against 500 kg load. As it is expected, stress was mostly occurred in the opposite side from load and top

supports of space frame which is shown in Figure 48. For simulation of dynamic load situation 1000 kg load was also applied. Stress was increased to 170 MPa against 1000 kg. Stiffness energy was also increased from 87 to 350 joule.
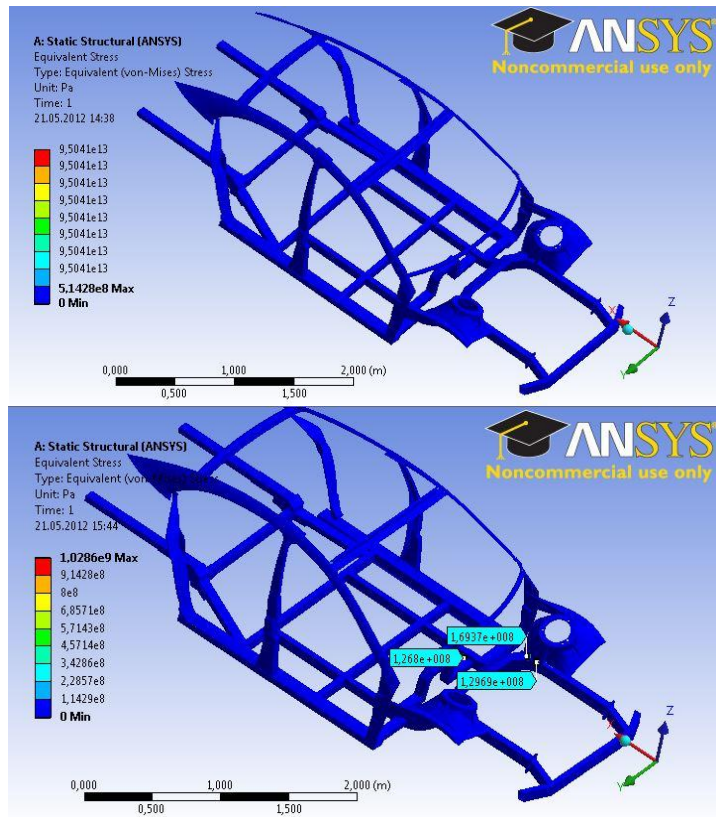
Figure 48: Equivalent Von – Mises stress results to simulate single wheel fall into one pit a) at 500 kg and b) at 1000 kg

When considering the fatigue life and damage in constant amplitude with proportional loading, critical parts were taken more damage with increasing load. The fatigue life was calculated as 10^8 and 5.6334×10^5 against 500 kg and 1000 kg respectively at the minimum point. It is not surprising that safety factor was decreased with increasing load. Regions that were exposed the maximum stress became approximately 0.5 factor against 1000 kg but other regions were still over critical limit which is 1.5. If the real-life situation is taken into account, a single wheel is never subjected to 1000 kg load when the total weight of car is

approximately 1500 kg. So the safety factor results of 1000 kg can be ignored and on the other hand factors will be increased with other sheet parts addition.

In constant amplitude with non – proportional loading analysis, stress was reached 200 MPa at maximum which was critical for space frame. This situation was simulated when an extra 500 kg load (totally 1000 kg) applied to the shock absorber that was already subjected to 500 kg load as an initial condition. On the other hand safety factor was determined under 1.5 in some points that can cause damage (see Figure 49). When compare with proportional loading, fatigue damage points and areas were decreased. While the lowest safety factor area 0.04 at proportional loading, it was increased to 0.09 at non – proportional loading. As it was mentioned before with the sheet panels and other parts addition, safety factor will be also increased. But this analysis shows us despite the opposite points of added load was critical; the majority of body had high safety factor.
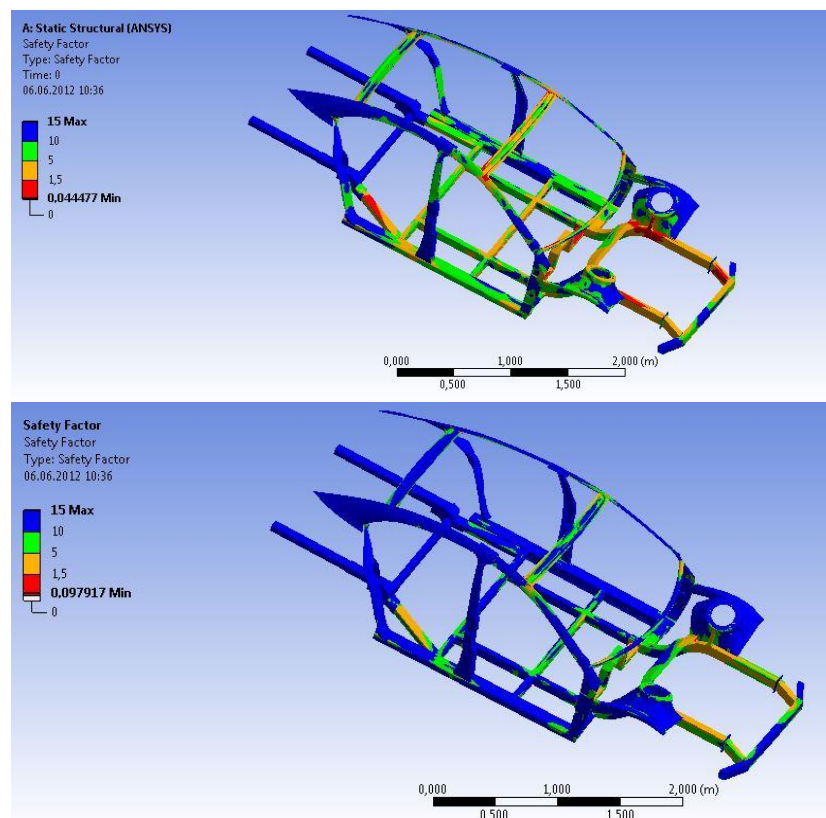
Figure 49: Safety factor results of constant amplitude proportional and non – proportional loading fatigue analysis

74

The analysis of individual parts such as B- pillar and shock absorber tower was also carried out. For B- Pillar (see Figure 50), there was not any critical stress determined in all body at 500 kg. Only in the middle point of pillar was reached to the damage point with maximum stress of 97 MPa at 500 kg. After 1000 kg load was applied the some points of the pillar was exceed the damage limits and stresses were determined above 200 MPa. For shock absorber tower (see Figure 51), forces were applied to the connection holes and stresses were determined approximately 100 MPa and 160 MPa against 500 kg and 1000 kg loads respectively. Stresses were below the plastic deformation region but some points around the holes were above the damage limit. Both parts were strong enough against 500 kg loads and the majority of bodies were under critical limits at 1000 kg.
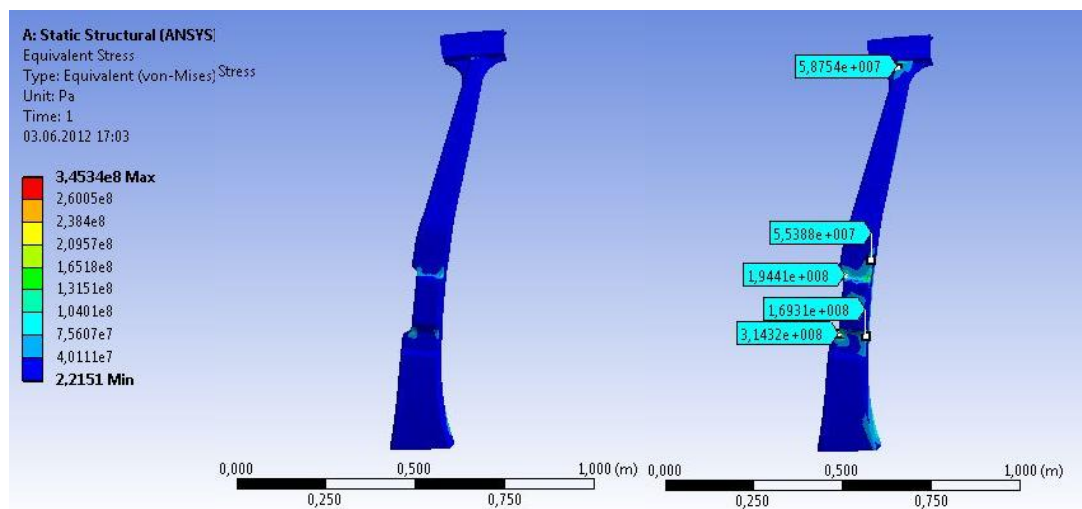
Figure 50: Equivalent stress distribution of B – Pillar against a) 500 kg and b) 1000 kg load
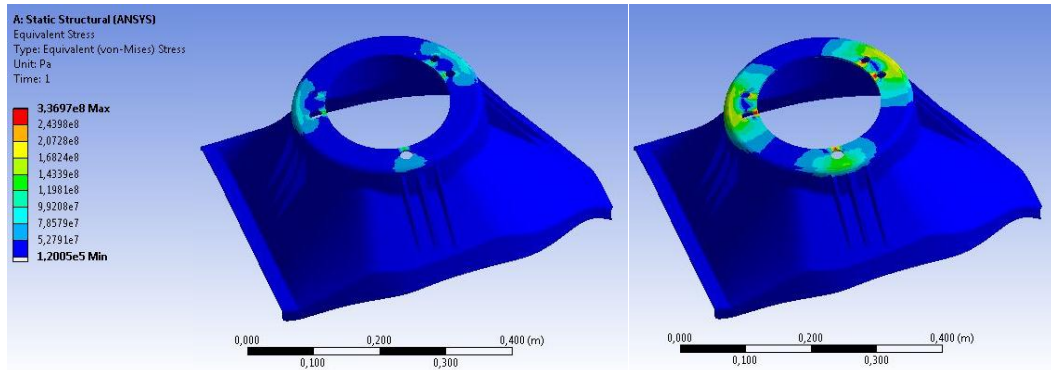
Figure 51: Equivalent stress distribution of shock absorber against a) 500 kg and b) 1000 kg load

First method for rare joint parts was done with 500 kg load and results are shown in Figure 52. Equivalent (Von – Mises) stress distribution and total deformation results were determined. Stress value was not high before and after the strengthening the joint areas so it was not critical. In comparison of total deformation, while the profile in the middle was deformed totally, after strengthening deformation value was decreased and distributed more uniformly.
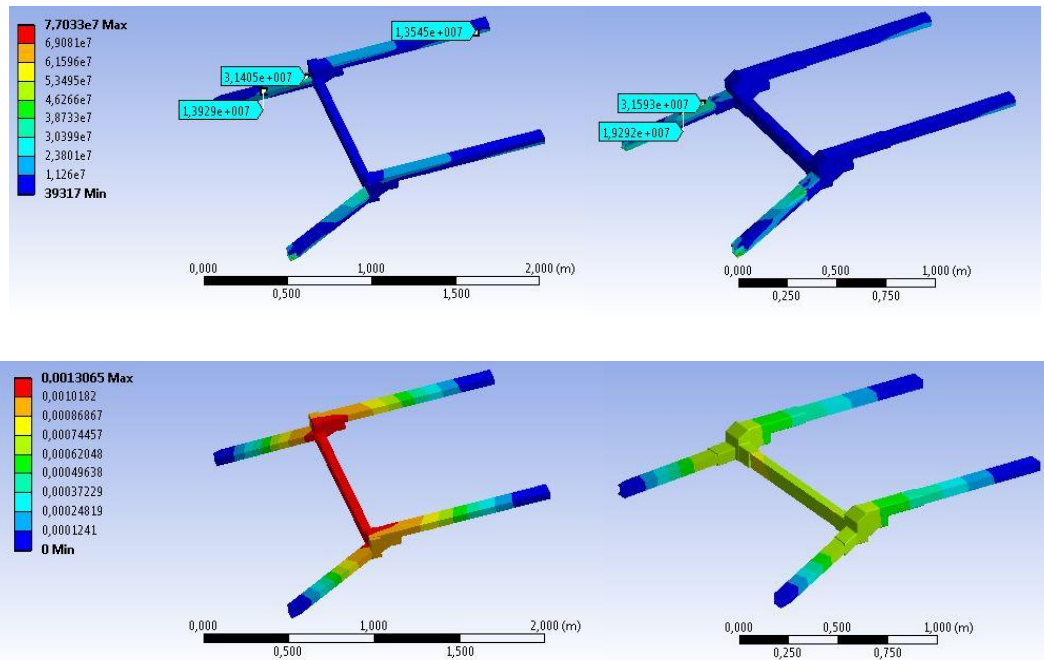
Figure 52: Comparison of equivalent stress distribution and total deformation of unsupported (left) and supported (right) joint parts after 500 kg loads were applied to each joint point

The analysis results of 1000 kg when load was applied to the one mounting location to simulate the single wheel fall into pit, is shown in Figure 53. The overall stress results were increased in both design but the stress distribution was in more limited area when the joint was supported with casting part as it was expected. It was observed that support was not effective in maximum stress. But deformation was decreased again and became more uniform with the strengthening.
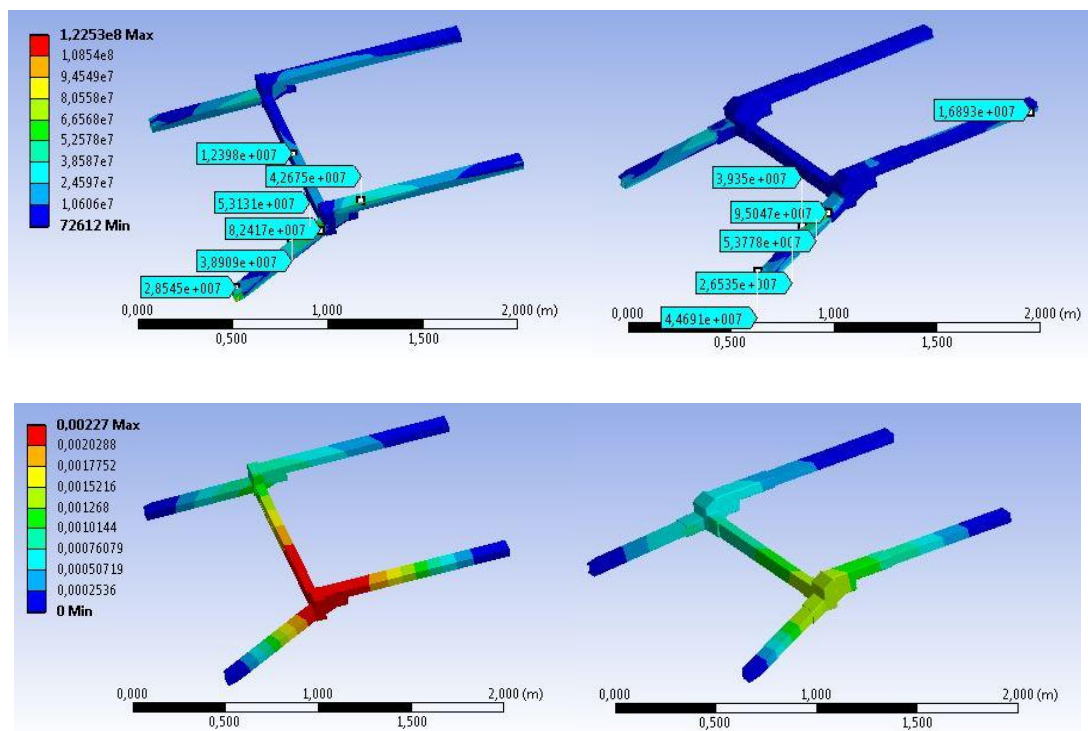
Figure 53: Comparison of equivalent stress distribution and total deformation of unsupported (left) and supported (right) joint parts while 500 kg was applied to the left joint point and 1000 kg to the right

Besides the results were not surprising after strengthening, the efficiency with increasing mass was more important. In this reason, stiffness, stiffness energy and efficiency were compared. Efficiency was calculated with the total mass was divided by the stiffness and results are written on Table 25. The stiffness of supported part was higher than the unsupported joint area and the consumed stiffness energy against force was less. The efficiency was also increased as 6.58% against 500 – 500 kg load

and 1.15% against 500 – 1000 kg load. Results show that strengthening has a positive effect on stress and deformation in rare area, even the total mass was increased supported joint parts were still more efficient for stiffness.

Table 25: Stiffness and efficiency results of unsupported and supported rare parts

	Without Support		With Support	
Load (Kg)	500 – 500	500 - 1000	500 – 500	500 - 1000
Mass (Kg)	19,982	19,982	32,097	32,097
Stiffness Energy (J)	4,8678	12,621	3,2127	8,0749
Stiffness (N.m / deg)	4111,547	4028,393	6196,172	6396,952
Efficiency (g / Nm/ deg)	4,859971	4,96029	5,180133	5,017546

4.4.2 Dynamic Analysis
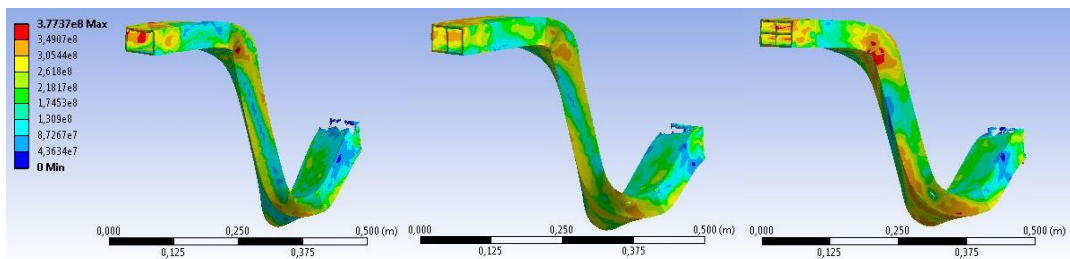
Figure 54: Comparison of equivalent stress of aluminum profiles that have different cross – sections in impact analysis

Figure 54 shows the deformed profiles that have different cross – sections after 0.05 seconds. The highest stress was determined from the folding points and the stress distribution of all profiles was almost same. The energy absorption was determined from the kinetic energy loss of rare load which was initially bonded to the profile. Also the specific energy absorption of each profile was calculated (total absorbed energy / total mass of profile) and all results are given in Table 26. As it is seen from the table, energy absorption was increased with reinforcements as it was expected. When compared the energy absorptions with the empty cross – section, single

supported profile was absorbed 30.5% and double supported profile was absorbed 53.7% more energy. Despite the double supported profile was absorbed the highest energy with 21kJ, specific energy absorption (SEA) results was found differently. Because when the mass was considered, the heaviest profile was double supported profile and thus the specific energy absorption was not determined as high as single supported profile. Reinforcement was increased the specific energy absorption when comparing with the empty cross – section, as 12.5% in single supported profile. Consequently, while the mass was increased with the absorbing energy, single supported profile was found the most efficient cross- section between these three candidates.

Table 26: Energy absorbance and specific energy absorbance results of S-shaped

Cross – Section Type	Mass (g)	Energy Absorption (J)	SEA (J/g)	Peak Force (kN)
Empty	2133,3	14131	6,6	98,02
Single Supported	2483,3	18450	7,43	99,63
Double Supported	3056,8	21721,3	7,1	105

Besides the energy absorption and the specific energy absorption results, peak forces are also important which is undesirable. The force – time curve of each cross - section is shown in Figure 55. According to the peak forces results which are given in Table 26 while the energy absorption was increasing with reinforcing the profiles, it also increases the peak forces. In order to prevent the transfer of force to the occupants in a frontal crash, lower peak forces were desired. All peak force results were determined close to the each other and empty profile had the minimum peak force as it was expected. Also the peak force of single supported profile was much the same as empty profile. When the energy absorption was also taken into account, single supported profile was given the optimum results despite increasing in peak force compared to empty aluminum profile.
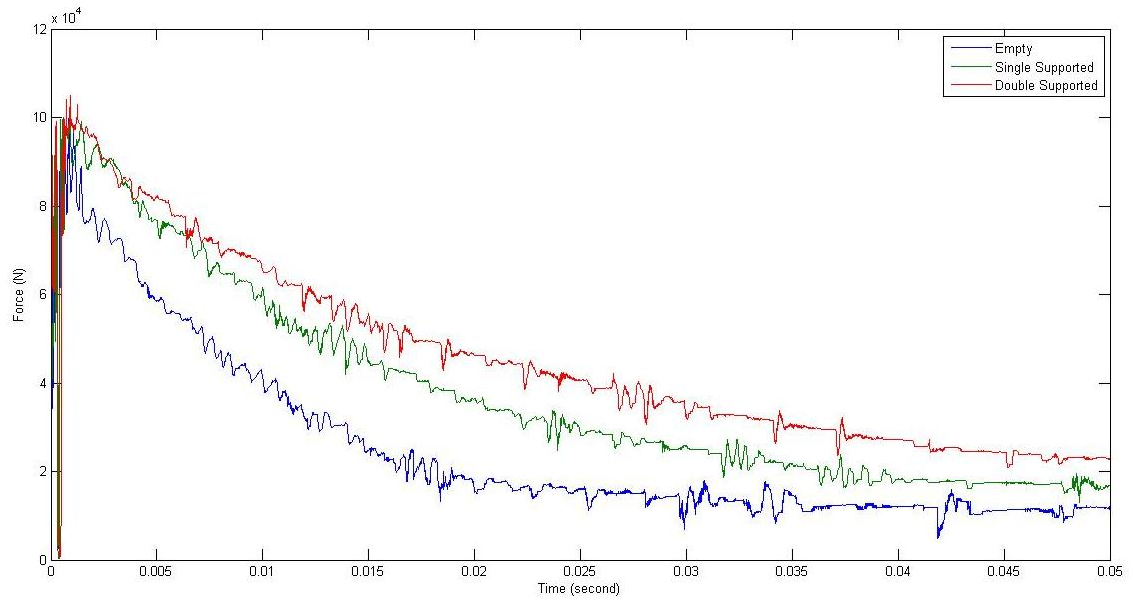
Figure 55: The force – time curve of s-shaped profiles for 0.05 seconds that were impacted to a rigid wall

CHAPTER 5

CONCLUSIONS

In the present study, many investigations were done to produce a precise aluminum space frame chassis; chassis calculations, design optimization, static and dynamic load effects on chassis, proper alloy and process selection, production and mechanical evaluations. The goal was achieved according to the results of the study and the feasibility of the production of a lightweight chassis was understood. The manufactured chassis was put into practice for the production of an automobile with some additions and modifications, during time this thesis was being written. The following conclusions can be drawn after investigations.

1- *The most suitable alloy for thin-walled and complex parts with sufficient mechanical properties was found as Silafont – 36.* Spiral fluidity test results gave two candidate aluminum alloys (A356.0 and Silafont – 36) according to their high castability for thin sections. In comparison of mechanical properties between Silafont – 36 and A356.0, the higher ultimate tensile strength ($\approx$200 MPa) and elongation ($\approx$4%) were found at Silafont – 36 aluminum alloy.

2- *In alloy preparation, grain refinement and modification of Al – Si alloy was done succesfully in sand casting.* According to the thermal analysis results, liquidus undercooling was getting smaller with grain refinement addition. Also the eutectic undercooling was suppressed by 2.9 ºC and solidification time was increased. Light microscopy images were proved the sufficient modification with the spherical Si particles.

3- *Artificial aging (T6) heat treatment has given the optimum results in mechanical evaluations for sand cast Silafont – 36 aluminum alloy.* Hardness

test was done to identify the proper solutionizing and artificial aging time; 3 hours at 490 ºC and 6 hours at 170 ºC was found respectively. In comparison of tensile test results, while the T6 heat-treated aluminum samples were given the highest ultimate tensile strength (≈205MPa), the highest (≈5%) elongation was found in the annealed samples. In order to determine the energy absorbance results, charpy impact test was done and the most energy absorption (≈14j) was observed in T4 heat-treated samples.

4- *For artificial aging of extrusion profiles, sufficient hardness (73.1 HB) was obtained by aging process for 6 hours at 185 ºC.* Heat treatment (T6) of extrusion samples was done in several times from 2 to 20 hours. On the other hand, another heat treatment (T5) was also carried out in higher temperature at 205 ºC but hardness was determined lower than T6. The maximum hardness (≈56HB) was determined at 2 hours at this temperature.

5- *The highest peak load (85kN) and energy absorption (4927j) results were determined in T6 heat-treated aluminum extrusion profile in three point bending test.* According to compensate the steel profile in chassis, the design and the thickness was changed in aluminum profile. The ultimate tensile strength and yield strength were observed highest in heat-treated aluminum profile. The maximum elongation (20%) was found in untreated aluminum profile. But while the visible cracks and fractures were occurred underneath the upper intender in parallel direction at untreated aluminum and low carbon steel profiles, the fracture was occurred perpendicular to the extrusion direction in heat-treated aluminum profile because of high stress intensity by support part. This support part was added shear stress to the profile in high static flexural loads.

6- *Due to changes in dimension and thickness of cross-sections, aluminum profiles can be replaced with the steel frames.* In calculation of moment of inertia, the higher inertia values was determined in aluminum (413501 mm^4) compared to steel (179114.58 mm^4). If the elastic modulus and inertia results were considered together, aluminum was given similar values as steel in safety region. The ultimate tensile strength results were also similar but the yield strength of aluminum profile was lower as it was expected. Decreasing

in yield and ultimate tensile strength was observed, when the shear stress was also considered.

7- *Mechanical properties of extruded and sand cast samples were lowered after welding.* Hardness of heat treated samples was reduced at the heat affected zone. HAZ was continued approximately 20 mm away from welding pool in extruded samples and 18 mm in sand cast samples. Also hardness was increased when a period of time passed with the help of natural aging. This increment was occurred in a shorter time at the same situation under the sunlight but it is not too efficient. The hardness of weld seam in sand cast samples was higher than the extruded samples owing to the high silicon content of sand casting alloy. In tensile tests, while fracture was occurred in weld seam at extruded samples, it was occurred in parent metal in sand cast samples. This result was observed because of the changing in silicon content at welding pool. Ultimate tensile strength and elongation was higher in sand cast samples ($\approx$116 MPa, $\approx$5.5%) than the extruded samples ($\approx$97MPa, $\approx$3.7%)

8- *The designed space frame was given sufficient stiffness at 2000 kg against bending static loadings simulated by finite element analysis.* Despite some areas were under safety factor, it will be increased with the addition of sheet metals. The individual parts as shock absorber and B – pillar was analyzed against 500 and 1000 kg loads. Both parts were strong enough against 500 kg loads and the majority of bodies were under critical limits at 1000 kg.

9- *Torsional stiffness was increased with the applied load as it was expected and determined as 5153.872 Nm/deg.* Damage was not occurred below 4000 N.m torque and torsional stiffness was found under typical vehicles because of many parts were missing.

10- *Fatigue life was decreasing with increasing torsional loading but the majority of body was above safety factor.* In comparison of proportional and non-proportional loading with constant amplitude, fatigue damage was decreased and safety factor was increased with the loading change. Damage areas were reduced with the proportional loading.

11- *The weak rear joint parts of space frame were strengthened efficiently.* A cast support part was added to the weak joint area to reduce the total deformation.

But support part was not significantly effective on maximum equivalent stress. Despite increasing stiffness with an increasing weight, strengthened area with cast part was still more efficient compared to the unsupported area.

12- *Single supported s-shaped extrusion profile was given the optimum results at dynamic analysis*. While the energy absorption was increased with increasing reinforcement, specific energy absorption was observed highest in the single supported profile due to its lower mass than the double supported profile. Also peak forces were determined close to the each other in all cross – sections (≈100kN).

REFERENCES

[1]   F.G. Armao, "*Design and Fabrication of Aluminum Automobiles,*" Welding Innovation, vol. 19, no. 2, pp. 1-5, 2002

[2]   W.Paatsch, "*Recent Trends in Surface Finishing for Automobile Industry in Germany,*" Surface and Coatings Technology, vol. 169-170, pp. 753-757, Jun. 2003

[3]   W.S. Miller, L. Zhuang, J. Bottema, A.J. Wittebrood, P. De Smet, A.Haszler, A. Vieregge, "*Recent Development in Aluminum Alloys for the Automotive Industry,*" Materials Science and Engineering, vol. A280, pp. 37-49, 2000

[4]   M.Saito, "*Development Aluminum Bodies for Fuel Efficient Vehicles,*" Materials Today, pp. 30-34

[5]   The Aluminum Association, "*Aluminum Automotive Extrusion Manual,*" Publication AT6, Washington, pp. 2-11, Dec. 1998

[6]   J.Zahnder, R. Pritzlaff, S. Lundberg, B. Gilmont, "*Aluminum in Commercial Vehicles,*" European Aluminum Association, pp. 57 – 89

[7]   The Aluminum Association, "*Aluminum: The Corrosion Resistant Automotive Material,*" Publication AT7, pp. 10-15, May 2001

[8]   A. Deb, M.S. Mahendrakumar, C. Chavan, J. Karve, D. Blankenburg, S. Storen, "*Design of an Aluminum-Based Vehicle Platform for Front Impact Safety,*" International Journal of Impact Engineering, vol. 30, no. 8-9, pp. 1055-1079, Oct. 2004

[9]   D. Carle, G. Blount, "*The Suitability of an Aluminum as an Alternative Material for Car Bodies,*" Materials and Design, vol. 20, no. 5, pp. 267-272, Oct. 1999

[10]   V.S. Zolotorevsky, N.A. Below, M.V. Glazoff, "*Casting Aluminum Alloys,*" Elsevier, Great Britain, pp. 45-47, 2007

[11]   J.G. Kaufman, E.L. Rooy, "*Aluminum Alloy Casting: Properties, Process and Applications,*" ASM International, pp. 39-67, Dec. 2004

[12] Aluminium Rheinfelden GmbH, *"Silafont – 36: Primer Aluminum Injection Casting Alloy,"* vol. Sf-36/518, pp. 1-12, 2003

[13] D.G. Altenpohl, *"Aluminum: Technology, Applications and Environment,"* Aluminum Association, Minerals, Metals and Materials Society, pp. 120-373, 1998

[14] J.R. Davis, *"Alloying Understanding the Basics,"* ASM International, pp. 367-385, 2001

[15] D.S. Mackenzie, E.G. Totten, *"Handbook of Aluminum: Physical Metallurgy and Process,"* Marcel Dekker Inc., New York, vol. 1, pp. 259-643, 2003

[16] F. Baypınar, *"Grain Refining of Aluminum Foundry Alloys using Al5Ti1B,"* M.Sc. Thesis, Graduate School of Natural and Applied Science of Gazi University, pp. 2-18, Dec. 2005

[17] A.Rashid, *"The Treatment of Liquid Aluminum – Silicon Alloys,"* Lecture 17, Department of MME, BUET, Daka, pp. 1-15, 2010

[18] Aluminium Rheinfelden GmbH, *"Primer Aluminum Casting Alloys,"* Version 7, pp. 80-118, 2010

[19] R. Kayıkçı, M. Çolak, *"Grain Refinement in Aluminum Casting,"* Journal of Science of Sakarya University, vol.13, no.1, pp. 11-17, 2009

[20] S. Nafisi, R. Ghomashchi, *"Grain Refining of Conventional and Semi-Solid A356 Al-Si Alloy,"* Journal of Materials Processiong Technology, vol. 174, no. 1-3, pp. 371-383, May 2006

[21] R.Cook, *"Grain Refinement of Aluminum – Silicon Foundry Alloys,"* Metallurg Aluminum, pp. 1-19, 1998

[22] M.Tutar, *"Alüminyum Döküm Alaşımları,"* Lecture Notes, Mechanical Engineering of Uludag University, pp. 106 -112, 2010

[23] H.V. Guthy, *"Evolution of the Eutectic Microstructure in Chemically Modified and Unmodified Aluminum Silicon Alloys,"* M.Sc. Thesis, Master of Science of Worcester Polytechnic Institute, pp. 23-47, 2002

[24] T. Ulucak, *"Metallurgy of AA 6063 Aluminum Alloy",* http://www.aluminyumsanayi.com/6063metalurji.htm, last visited August 2012

[25] E. Demir, *"Investigation of the Heat Treatment Effects on Aluminum Alloys,"* M.Sc. Thesis, Graduate School of Natural and Applied Science of Dokuz Eylul University, pp. 6-34, Dec. 2008

[26] H. Chandler, *"Heat Treater's Guide: Practices and Procedures for Nonferrous Alloys,"* ASM International, pp. 131-145, 1996

[27] D.A. Crolla, *"Automotive Engineering: Powertrain, Chassis System and Vehicle Body,"* Butterworth – Heinemann, Oxford, pp. 525 – 591, 2009

[28] H.S. Kim, *"New Extruded Multi-Cell Aluminum Profile for Maximum Crash Energy Absorption and Weight Efficiency,"* Thin-Walled Structures, vol. 40, no. 4, pp. 311-327, Apr. 2002

[29] T. Paananen, *"Design and Dynamic Analysis of a Space Frame for Acoustic Measurements,"* M.Sc. Thesis, Master of Science in Mechanical Engineering of University of Karlskrona/Ronneby, pp. 13-25, 1998

[30] J. Helsen, L. Cremers, P. Mas, P. Sas, *"Global Static and Dynamic Car Body Stiffness Based on a Single Experimental Modal Analysis Test,"* Modal Testing: Methods and Case Studies, pp. 2505-2522, 2012

[31] P.J. Cunat, *"Stainless Steel Properties for Structural Automotive Applications,"* Metal Bulletin International Automotive Materials Conference, Cologne, pp. 1-10, Jun. 2000

[32] H.S. Kim, T. Wierzbicki, *"Effect of the Cross-Sectional Shape of Hat-Type Cross-Sections on Crash Resistance of an "S"- Frame,"* Thin-Walled Structures, vol. 39, pp. 535-554, Mar. 2001

[33] C. Zhang, A. Saigal, *"Crash Behavior of 3D S-Shape Space Frame Structure,"* Journal of Materials Processing Technology, vol. 191, pp. 256 – 259, 2007

[34] F.A. Mohamed, *"On Creep Behavior in Powder Metallurgy 6061 Al,"* Scripta Materiala, vol. 38, no. 5, pp. 457-463, 1998

[35] D.A. Hancq, *"Fatigue Analysis in the Ansys Workbench Environment,"* Ansys Inc., pp. 1-31, May 2003

[36] Aluminum Company of America, *"Welding Alcoa Aluminum,"* pp. 29-63, 1967

[37] K.Yurtışık, M.Ekşi, C.Batıgün, *"6063 ve 5754 Kalitelerindeki Aluminyum Alaşımlarının Değişen Alaşım İlavesi ve Darbeli Akım Gaz-Altı Ark Yöntemiyle Kaynaklanabilirliği",* Savtek Savunma Teknolojileri Kongresi, Ankara, 2010

[38] Kaiser Aluminum Staff, *"Kaiser Aluminum Welding,"* California, pp. 2.30 – 9.10, 1967

[39] J.Dwight, *"Aluminum Design and Construction,"* E &FN Spon, New York, 1999

[40]   N.R. Mandal, *"Aluminum Welding,"* ASM International, 2nd Edition, pp. 9-103, Feb. 2006

[41]   C.Odabaş, *"Aluminyum ve Alaşımlarının Kaynağı,"* Askaynak, pp. 1-3, 2007

[42]   J.R. Davis, *"Concise Metals Engineering Data Book,"* ASM International, Ohio, pp. 69-70 Mar. 2009

[43]   A.Kielbus, *"The Influence of Casting Temperature on Castability and Structure of AJ62 Alloy,"* Achieves of Materials Science and Engineering, vol.28, no. 6, pp.345-348, Jun 2007

[44]   Unalloyed Primer Aluminum Products, http://www.etialuminyum.com, Eti Aluminyum, last visited on September 14, 2012

[45]   ASTM, *"Standard Practice for Verification of Test Frame and Specimen Alignment under Tensile and Compressive Axial Force Application,"* American Society for Testing and Materials, E1012-05, pp. 1-11, 2005

[46]   ASTM, *"Standard Test Methods for Notched Bar Impact Testing of Metallic Materials,"* American Society for Testing and Materials, E23 REV A, pp.1-28, 2007

[47]   ASTM, *"Standard Practice for Heat Treatment of Wrought Aluminum Alloys,"* American Society for Testing and Materials, B918/B918M, pp. 1-14, 2009

[48]   T.Korad, J.T.H. Pearce, M.Ponboon, U. Phongsophhitanan, *"Quantification of Precipitated Phases in 6063 Aluminum Billet by Image Analysis for Improvement of Homogenization Condition,"* Journal of Chemical Engineering and Applied Chemistry of Thailand, pp. 1-3

[49]   DIN, *"Destructive Testing of Welds in Metallic Materials – Transverse Tensile Test,"* Deutsches Institut Fur Normung E.V., EN 895, pp. 1-14, 1999

[50]   ASTM, *"Standard Test Methods for Bend Testing of Material for Ductility,"* American Society for Testing and Materials, E290, pp. 1-10, 2009

[51]   A.Ockewitz, D.Z. Sun, *"Damage Modelling of Automobile Components of Aluminum Materials under Crash Loading,"* LS-DYNA Andwenderforum, Ulm, pp. 1-12, 2006

[52]   D.Varas, R. Zaera, J.Lopez-Puente, *"Numerical Modeling of the Hydrodynamic Ram Phenomenon"*, International Journal of Impact Engineering, vol.36, no.3, pp. 363-374, 2009

[53]   D.C. Tyrell, K.J. Severson, B.P. Marquis, *"Analysis of Occupant Protection Strategies in Train Collusions"*, Crashworthiness and Occupant Protection in Transportation Systems, ASME, AMD vol. 210/BED vol. 30, pp. 1-19, 1995

[54]   A. Niklas, U. Abaunza, A.I. Fernandez-Calvo, J. Lacaze, R. Suarez, *"Thermal Analysis as a Microstructure Prediction Tool for A356 Aluminum Parts*

Solidified Under Various Cooling Conditions," The 69th WFC Paper, vol. 8, no. 1, pp. 89-95, Feb. 2011

[55]   J.G. Kaufman, "*Aluminum Alloy Database,*" Knovel, online source at http://www.knovel.com/web/portal/browse/display?_EXT_KNOVEL_DISPL AY_bookid=844&VerticalID=0, 2009, last visited on September 14, 2012

[56]   J.R. Davis, "*Corrosion of Aluminum and Aluminum Alloys*", ASM International, pp. 99-117, 1999

APPENDIX A

CHARPY IMPACT TEST SAMPLE PHOTOS

Figure 56: Broken Charpy impact test samples. (From top to bottom) T6 heat treated sample, T4 heat treated sample, annealed heat treated sample and untreated sample

APPENDIX B

3 – POINT BENDING TEST SAMPLES PHOTOS

Figure 57: Deformed 3 – point bending samples. (From top to bottom) T6 heat treated aluminum profile, T4 heat treated aluminum profile, low carbon steel profile

APPENDIX C
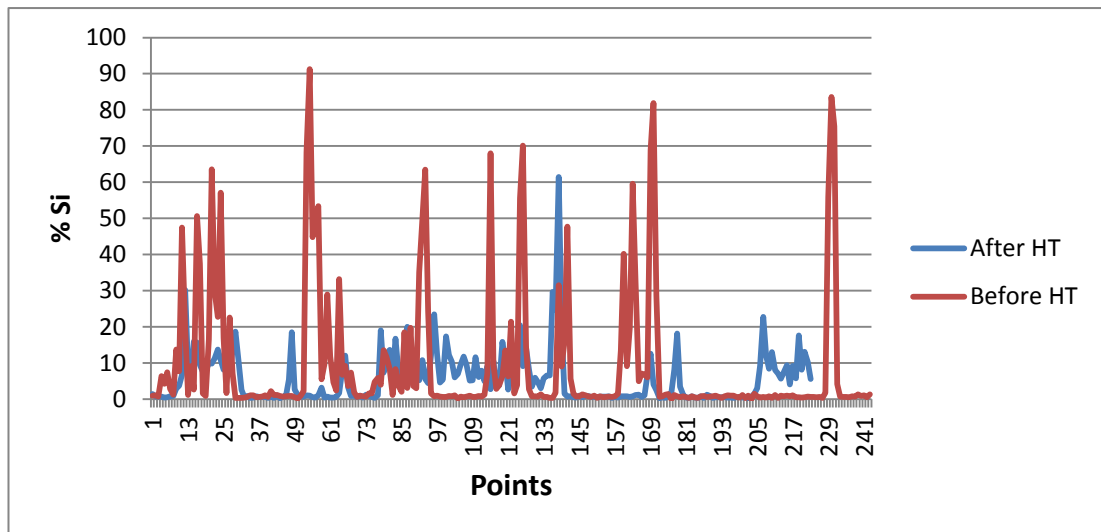
EDX LINE SCAN IN DENDRITES AFTER HEAT TREATMENT

Figure 58: Comparing %Si content in dendrites after heat treatment by EDX line scan

APPENDIX D

DESIGN AND FINAL VIEWS OF AUTOMOBILE

Figure 59: Design and final views of manufactured automobile in this study